

# Prospects for AGN studies with ALMA

R. Maiolino

*INAF - Astronomical Observatory of Rome*

---

## Abstract

These lecture notes provide an introduction to mm/submm extragalactic astronomy, focused on AGN studies, with the final goal of preparing students to their future exploitation of the ALMA capabilities. I first provide an overview of the current results obtained through mm/submm observations of galaxies and AGNs, both local and at high redshift. Then I summarize the main mm/submm facilities that are currently available. ALMA is then presented with a general description and by providing some details on its observing capabilities. Finally, I discuss some of the scientific goals that will be achievable with ALMA in extragalactic astronomy, and for AGN studies in particular.

*Key words:* galaxies: active, evolution, formation, high-redshift, nuclei, quasars, Seyfert, starburst, millimeter, submillimeter, instrumentation: high angular resolution, interferometers

*PACS:* 95.85.Fm, 95.85.Bh, 98.54.-h, 98.54.Cm, 98.54.Ep, 98.54.Kt

---

## 1 Introduction

The Atacama Large Millimeter Array (ALMA) is one of the largest ground-based astronomy projects of the next decade, which will revolutionize several fields of astronomy. A large community of scientists is expected to use ALMA to tackle several outstanding questions in astrophysics. However, mm/submm astronomy is often considered a field restricted to experts. In the case of students and young scientists in particular, the limited familiarity with mm/submm facilities and observations may prevent them to fully exploit the ALMA capabilities in the future. These lecture notes are aimed at providing students and young researches some background on mm/submm extragalactic astronomy, with a focus on the investigation of AGNs. I will first provide a quick overview of the current results obtained through extragalactic mm/submm observations, by focusing on AGNs (§2). I will then summarize the currently available (and forthcoming) mm-submm facilities (§3). Then I will shortly describe ALMA and summarize its observing capabilities (§4). Finally, I will

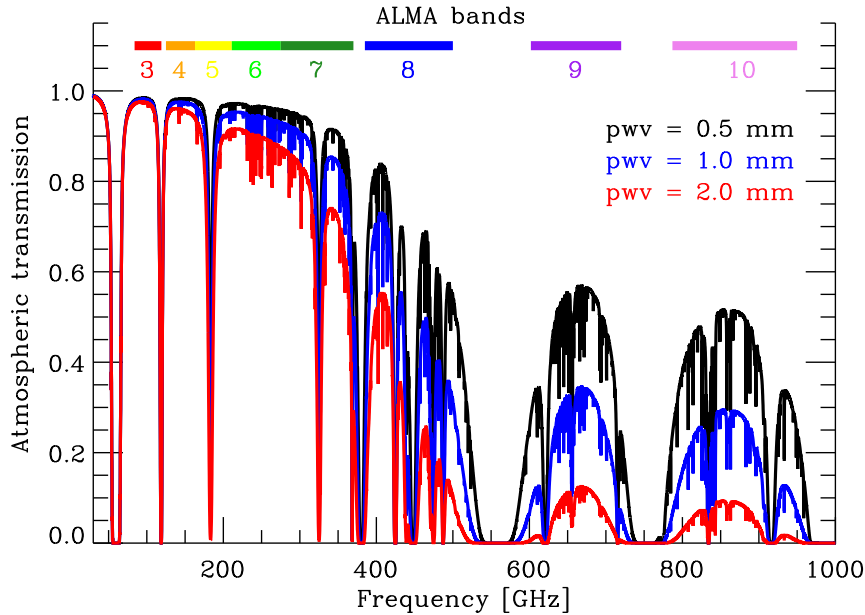


Fig. 1. Atmospheric transmission at Chajnantor Plateau, the ALMA site, with different amounts of precipitable water vapor. The horizontal colored bars indicate the frequency ranges of the ALMA bands.

discuss some of the ALMA prospects for extragalactic studies, and in particular for AGNs, both in the local universe and at cosmological distances (§5). These lecture notes are far from being exhaustive; several scientific cases will not be discussed at all; the main goal of these notes is only to provide an introduction to mm/submm extragalactic astronomy and to highlight some scientific cases that ALMA will be able to tackle.

## 2 Millimetric and submillimetric extragalactic astronomy

This branch of astronomy includes observations at wavelengths between  $\sim 10$  mm and  $\sim 300 \mu\text{m}$ . Longer wavelengths are traditionally identified as radio-astronomy domain. Shorter wavelengths, out to mid-IR wavelengths, are unobservable from ground because of the nearly complete atmospheric absorption (although some sites, under exceptional conditions, allow observations out to  $\sim 200 \mu\text{m}$ ). Even within the mm-submm range not all wavelengths are equally easy to observe, since the sky transparency on average decreases rapidly at shorter wavelengths. At  $\lambda < 700 \mu\text{m}$  only a few atmospheric windows are accessible, and only under optimal weather conditions. This issue is clearly illustrated in Fig. 1, which shows the atmospheric transmission at the ALMA site.

The main source of opacity at these wavelengths is the water vapor. This is the reason for locating mm-submm observatories at dry and high altitude sites,

where the amount of water vapor is much reduced. However, even at these optimal sites there are strong variations of the the water vapor, which make the atmospheric transmission change strongly (Fig. 1) both on long (seasonal) and short (day/night) time scales.

Given the difficulties of observing at these wavelengths one may wonder why international agencies are investing so much effort to develop facilities with enhanced observing capabilities in these bands. The mm-submm band contains a wealth of information that cannot be inferred from any other band. Most of the  $\sim 150$  molecules known so far in the *cold* interstellar medium (see <http://astrochemistry.net> for an updated list) emit their rotational transitions in the mm-submm bands, with a density of about 70 lines/GHz. All of these transitions are important diagnostics of the chemistry, of the physics and of the dynamics of the Inter Stellar Medium (ISM) from which stars form. Some of these lines are so strong (e.g. the CO transitions) to be powerful tools to trace the dynamics and the gas physics even in distant galaxies. Furthermore, some of the strongest lines emitted by the ISM of any galaxy, such as the [CII]158 $\mu\text{m}$  and the [OI]63 $\mu\text{m}$  fine structure lines (the two main coolants of the ISM), are redshifted into the mm-submm bands at  $z > 2-4$ .

Within the context of the continuum emission, the mm-submm bands encompass the Rayleigh-Jeans region of the warm dust thermal emission (which traces star formation and the dust mass), the high frequency tail of the synchrotron emission (dominating the radio emission in most galaxies) and of the free-free emission (tracing HII regions). At high redshift the prominent IR dust thermal bump (which dominates the Spectral Energy Distribution –SED– in starburst galaxies) is shifted into the submm band, therefore making this one of the best spectral regions to search and characterize high- $z$  star forming galaxies.

This was just a very quick glance at the scientific motivations behind the development of mm-submm facilities, and mostly limited to the extragalactic field. Young stellar objects, protostars and proto-planetary systems are, for instance, additional fields where the mm-submm range is crucial for a thorough investigation.

The importance of the mm-submm band within the extragalactic context will become more obvious in the following sections, where I will provide some (shallow) background on what we currently know of external galaxies based on mm-submm observations, and where some extragalactic ALMA science cases will be discussed.

On the technical side, it is important to mention that the (sub)mm is currently the shortest wavelength where sensitive, many-elements coherent detection interferometers are feasible from the ground. These can simultaneously

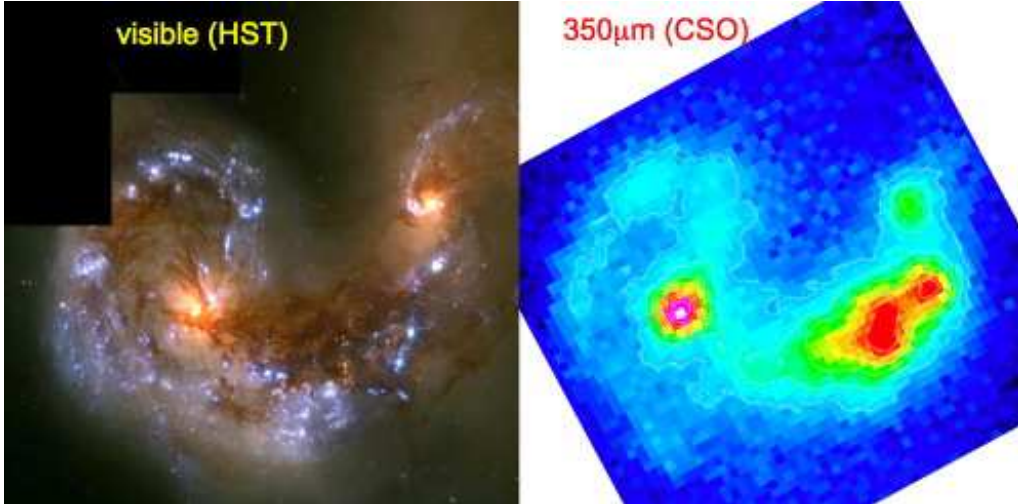


Fig. 2. Visible image of the interacting galaxies “Antennae” (*left*) compared with their submm image at  $350\mu\text{m}$  (*right*). Note that most of the far-IR emission comes from a region that is heavily obscured at optical wavelengths. Credit of the Space Telescope Science Institute (optical HST image) and of C. Dowell (submm CSO image).

provide high angular resolution, sensitivity, and image reconstruction fidelity. Direct detection interferometers at shorter wavelengths (e.g. mid/near-IR) can achieve similar angular resolution, but are more severely constrained in terms of sensitivity and image fidelity.

### 2.1 Local normal and starburst galaxies

The warm dust emitting at far-IR wavelengths is mostly heated by the UV radiation field of young massive stars in star forming regions. As a consequence, the far infrared luminosity  $L_{\text{FIR}}$  and its submm Rayleigh-Jeans part are considered good tracers of star formation in galaxies. In particular, these bands are useful to trace obscured star formation, since they are virtually unaffected by dust extinction. This is evident in Fig. 2, where the  $350\mu\text{m}$  map of the interacting galaxies “Antennae” (obtained at the CSO telescope, C. Dowell, priv. comm.) is compared with the optical HST image: the region of most vigorous star formation traced by the submm emission is actually the most obscured and less visible at optical wavelengths. The main problems of the current instrumentation (bolometer arrays on single dish telescopes) in tracing star formation in external galaxies are their limited sensitivity and their poor angular resolution ( $10''$ – $20''$ ). Both these issues will no longer be a problem with ALMA, which will have sensitivities orders of magnitude better and an angular resolution similar to HST.

As already mentioned, also most of the *gas* phase of the cold ISM emits in

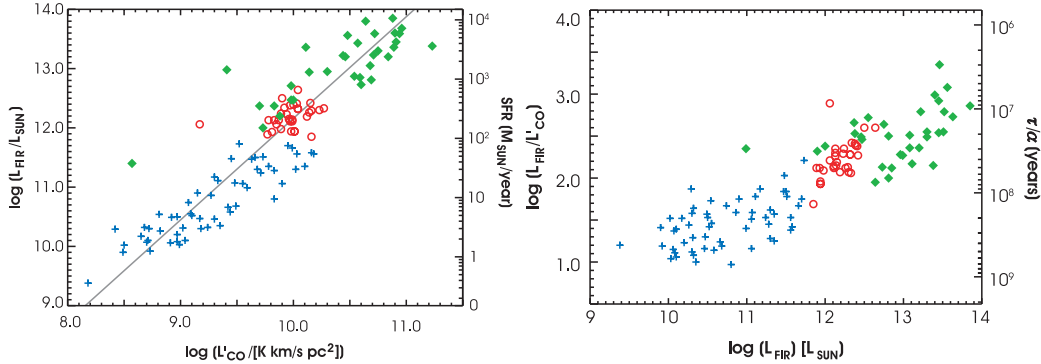


Fig. 3. *Left*: Relationship between far-IR luminosity and CO luminosity obtained for normal spirals (blue crosses), ULIRGs (red circles) and high redshift galaxies with CO detections (green diamonds). Note the non-linear relationship  $\log L_{\text{FIR}} = 1.7 \log L'_{\text{CO}} - 5.0$ , indicated by the solid line. The right-hand axis translates the far-IR luminosity into star formation rate. *Right*:  $L_{\text{FIR}}/L'_{\text{CO}}$  as a function of the far-IR luminosity. The right-hand axis gives the gas exhaustion timescale, where  $\alpha$  is the  $L'_{\text{CO}}$ -to- $\text{H}_2$  conversion factor ( $\alpha \approx 1 - 5 \text{ M}_{\odot} (\text{K km s}^{-1} \text{ pc}^{-2})^{-1}$ ). Both figures are from Solomon & Vanden Bout (2005).

the mm-submm range. More specifically, it is in this band that most of the molecular gas transitions are observed. However, *cold* molecular hydrogen  $\text{H}_2$  (by far the most abundant molecule in the cold gas phase) cannot be detected directly, since it has no electric dipole moment (therefore rotational transitions with  $\Delta J \pm 1$  are not allowed). Carbon monoxide CO is the second most abundant molecule: its rotational levels are excited by collisions with  $\text{H}_2$ , producing the brightest molecular lines in the spectrum of any galaxy. The luminosity of the CO rotational transitions, and in particular the fundamental one  $\text{J}(1 \rightarrow 0)$ , are widely used as tracers of the molecular gas mass through a linear relation:  $L_{\text{CO}} = \alpha M(\text{H}_2)$ . However, the conversion factor  $\alpha$  is found to depend on the gas metallicity as well as on its physical conditions (temperature and density).

The critical density of the CO transitions is relatively low, at least for the low rotational levels. For instance, the critical density of CO (1-0) (at 115 GHz) is about  $2 \cdot 10^3 \text{ cm}^{-3}$ . As a consequence, CO is generally little effective in tracing the high density regions of molecular clouds. Moreover, the large optical thickness the CO lines (at least for the low rotational levels) prevents us to penetrate dense molecular regions. Dense regions are better traced by other species, such as HCN,  $\text{HCO}^+$  and CS, which are characterized by higher critical densities for transitions in the same frequency bands as the CO ones. For instance HCN (1-0),  $\text{HCO}^+$  (1-0) and CS (2-1) (observable in the 3mm band), have critical densities of  $2 \cdot 10^6$ ,  $1.5 \cdot 10^5$  and  $4 \cdot 10^5 \text{ cm}^{-3}$ , respectively. However, these lines are typically one order of magnitude fainter than CO.

There is a relationship between infrared luminosity and CO luminosity, which is by itself not surprising (as most Luminosity-Luminosity relations). More interesting is the fact that the relation is not linear, being  $L_{\text{FIR}} \propto L'_{\text{CO}}{}^{1.7}$  (Fig. 3,

from Solomon & Vanden Bout (2005)). Since  $L_{\text{FIR}}$  is proportional to the star formation rate SFR, while  $L_{\text{CO}}$  is proportional to the molecular gas content  $M(\text{H}_2)$  (which is the fuel for star formation), the non linear relation implies that the star formation efficiency, defined as  $\text{SFE} = \text{SFR}/M(\text{H}_2)$  increases with the luminosity of the system. The inverse of the star formation efficiency is the gas exhaustion timescale,  $\tau = 1/\text{SFE} \propto L_{\text{CO}}/L_{\text{FIR}}$ , i.e. the time required by the starburst to totally consume the available molecular gas, if the star formation proceeds at the rate currently observed. The non-linear relation between  $L_{\text{FIR}}$  and  $L_{\text{CO}}$  implies that the gas exhaustion timescale decreases with luminosity, reaching values as low as  $10^7$ , as illustrated in Fig. 3. It is clear that the most powerful starbursts are also short lived. However, it should be mentioned that this picture may be biased, especially for what concerns high redshift sources, due to the incomplete census of galaxy populations. Indeed, Daddi et al. (2008) have recently identified some *powerful* starburst galaxies characterized by *low* SFE at  $z \sim 2$ .

The far-IR luminosity appears to be *linearly* correlated with the luminosity of dense gas tracers, such as HCN. The relation is linear over a very broad luminosity range spanning from Galactic star forming regions to powerful starburst galaxies (Wu et al., 2005). This result suggests that star formation always occurs in dense molecular clouds, and that star formation in starburst systems may simply be a scaled up version of Galactic star formation. However, also the linearity between  $L_{\text{FIR}}$  and  $L_{\text{HCN}}$  has been recently questioned through indications that the ratio between these two quantities increases with the luminosity (Graciá-Carpio et al., 2008). Moreover, the presence of an AGN may also affect the intensity of the HCN emission, as discussed in §2.2.

Interferometers allowed astronomers to map the molecular gas in large samples of galaxies, generally by exploiting the CO lines, but more recently also through transitions of various other species. The CO emission in galaxies show a variety of morphologies: spiral patterns, bars, rings, nuclear concentrations and irregular distributions (Helfer et al., 2003). The CO maps also reveal important kinematic information. In the case of disk or ring-like morphologies the gas kinematics is generally dominated by (nearly) regular rotation. In the case of barred galaxies, the molecular gas kinematics is often characterized by prominent streaming motions along the stellar bar (e.g. Regan et al., 1999; Schinnerer et al., 2007). This is regarded as direct evidence that the non-axisymmetric potential of a bar is effective in funneling gas into the central region (which may eventually produce a central starburst, or be further driven into the nuclear region to fuel an AGN).

## 2.2 Local AGNs

AGNs generally heat their circumnuclear dust to temperatures much higher than starburst galaxies. Indeed, active nuclei are generally characterized by strong mid-IR and near-IR emission, indicating dust temperatures of several hundred degrees and reaching the dust sublimation temperature (1500–2000 K). At far-IR and submillimeter wavelengths the relative contribution of AGN and star formation to the dust heating is debated. Spectral decomposition techniques, as well as the correlation between far-IR emission and other tracers of star formation, suggest that the far-IR and submm emission is dominated by star formation in the host galaxies, even in powerful QSOs (Schweitzer et al., 2006; Netzer et al., 2007). Disentangling *spatially* the far-IR/submm emission due to the AGN from the host galaxy emission is very difficult, if not impossible, with current facilities due to the lack of angular resolution at these wavelengths. Disentangling the two components is important not only to determine the contribution of AGNs to the far-IR/submm radiation, but also to constrain models of the obscuring dusty torus, as we shall see in §5.1.

Identifying the main mechanism responsible for fuelling AGNs has been one of the hottest topics in the last decade. Non-axisymmetric potentials introduced by stellar bars and galaxy interactions were considered as promising mechanisms, but various studies failed in finding any excess of these morphologies in AGNs. CO observations offer the possibility of directly witnessing the gas fuelling towards the nucleus. Intensive campaigns have been performed with millimetric interferometers to investigate this issue by mapping the CO emission in galaxies with different types of nuclear activity (e.g. the NUGA project, García-Burillo et al., 2005, 2007; Combes et al., 2004). The main result is that there is no evidence for systematic differences, in terms of molecular gas distribution and kinematics, between galaxies hosting AGNs and quiescent ones. In particular, Seyfert galaxies appear characterized by a wide variety of molecular gas distributions: streaming motions along stellar bars, rings, nuclear concentrations, nuclear voids and irregular distributions. The lack of any relationship between the presence of an AGN and the CO morphology/dynamics, indicates that there is no ubiquitous evidence for current fuelling of the AGN. One possibility, is that the large scale fuelling phase and the AGN phase may not be simultaneous. Another consideration is that local AGNs have low luminosities and do not require large fuelling rates from the host galaxies. More specifically, most local Seyfert nuclei are characterized by black hole accretion rates of about  $10^{-3} M_{\odot} \text{ yr}^{-1}$ ; at these rates even a single molecular cloud of  $10^6 M_{\odot}$  can keep the nucleus active for about 1 Gyr. The fuelling problem is more serious for powerful QSOs, where the accretion rates may exceed  $1 M_{\odot} \text{ yr}^{-1}$ . In QSOs some mechanism capable of funneling molecular gas from the host galaxy into the nuclear region is actually required. However, QSOs are

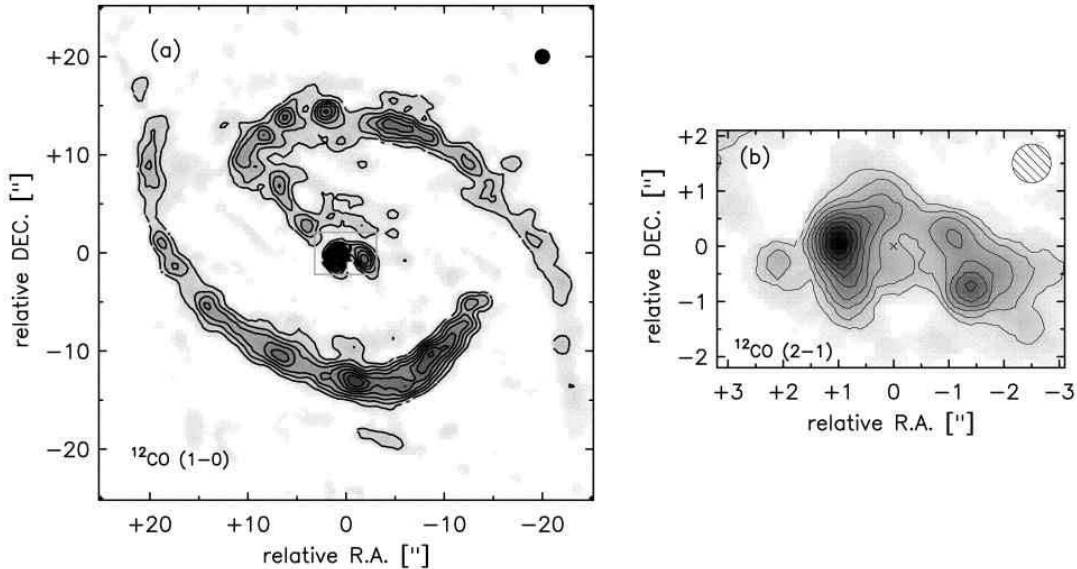


Fig. 4. *Left:* CO(1–0) interferometric maps of the Seyfert 2 galaxy NGC1068. *Right:* Zoom of the central region of the CO(2–1) map. The cross indicates the location of the radio nucleus. Circles at the top-left corner indicate the beam size. At the distance of NGC1068 one arcsec corresponds to about 80 pc. Both maps are from Schinnerer et al. (2000).

much more distant than Seyfert galaxies. The limited sensitivity and angular resolution of current mm interferometers hampers our capability of mapping the molecular gas distribution in QSO hosts, which will instead be easy with ALMA.

NGC 1068 is one of the best studied AGNs also at mm-submm wavelengths. At the highest resolution currently achievable the nuclear CO distribution shows a broken ring-like structure, about  $2''$  in size (corresponding to 140 pc), as illustrated in Fig. 4 (Schinnerer et al., 2000). At the specific location of the AGN (cross in Fig. 4) little CO emission is observed. Does this mean that little or no molecular gas is present in the vicinity of the AGN? This is somewhat contrary to expectations, given the need of gas in the vicinity of the AGN both to feed it and to provide the heavy obscuration characterizing NGC 1068 (Matt et al., 1997). Actually, we know that in the vicinity of the AGN, on scales of 1–10 pc, dense molecular gas and dust are present, based on radio and mid-IR interferometric observations (Greenhill et al., 1996; Jaffe et al., 2004). Possibly most of the molecular gas in the nuclear region is dense and warm, and therefore not properly sampled by the CO lines (at least not by the low rotational transitions). Maps of other lines tracing dense gas, such as HCN, have lower angular resolution (Tacconi et al., 1994), but do show a much higher concentration on the nucleus with respect to CO. Usero et al. (2004) detected several molecular species in the nucleus of NGC 1068 tracing not only dense gas, but also a very complex chemistry. These findings indicate that the AGN has created a giant “X-ray Dominated Region” (XDR).



Hard X-ray photons emitted by the AGN can penetrate deep into the circumnuclear molecular clouds and keep the temperature high over an extended region. The high gas temperature in XDR's favors the formation of various molecular species such as HCN (Maloney et al., 1996; Lepp & Dalgarno, 1996; Meijerink et al., 2007). In contrast, Photo Dissociation Regions (PDR), which are generated by the UV photons of star forming regions, are characterized by a much narrower region with enhanced temperature, making the production of various molecular species much less efficient than in XDR. These fundamental differences between XDR's and PDR's suggest that XDR-enhanced species can be used to unveil the presence of heavily obscured AGNs that escaped detection at other wavelengths. Within this context Graciá-Carpio et al. (2006) and Kohno et al. (2008) developed a diagnostic diagram involving the line ratios  $\text{HCN}/\text{HCO}^+$  versus  $\text{HCN}/\text{CO}$ , where pure Seyfert nuclei are clearly separated from starburst nuclei, in the sense that the former show enhanced HCN emission (but see also caveats discussed in Papadopoulos, 2007). This and other complementary diagnostic diagrams will be usable with ALMA to identify obscured AGNs even in distant galaxies.

### 2.3 Distant starburst galaxies

As the spectrum of a starburst galaxy moves in redshift, the global flux is reduced according to the  $1/D^2$  cosmological dimming, but the intrinsic luminosity observed at a fixed mm-submm wavelength increases as a consequence of the steeply rising submm continuum. At  $z > 1$  such strong negative K-correction counteracts completely the cosmological dimming, so that detecting a source at  $z=10$  is as easy as detecting a source at  $z=1$  (for a given intrinsic luminosity). This effect is illustrated in Fig. 5, which shows the observed flux distribution of a star forming galaxy at different redshifts. The flux observed at  $\lambda_{obs} = 1$  mm is essentially unchanged within the redshift range  $z \sim 1 - 10$ . Fig. 6 shows the same effect by plotting, for a given starburst template, the observed flux at various wavelengths (and specifically in the ALMA bands) as a function of redshift. The observed flux remains nearly constant in the redshift range  $1 < z < 10$  at wavelengths longer than about  $800 \mu\text{m}$ . At wavelengths shorter than  $\sim 500 \mu\text{m}$  the K-correction is not strong enough to compensate for the cosmological dimming. At wavelengths longer than  $\sim 2$  mm the K-correction is strong, but the observed flux is more than one order of magnitude fainter than observed at 1 mm; moreover, at  $\lambda > 2$  mm there is an increasing "risk" of contamination by non-thermal sources.

An interesting consequence of the strongly negative K-correction at mm-submm wavelengths is that in any deep field one expects to see many more galaxies at  $z > 1.5$  than at lower redshifts. This is just the opposite of what observed in the optical, where the distribution of observed fluxes is dominated

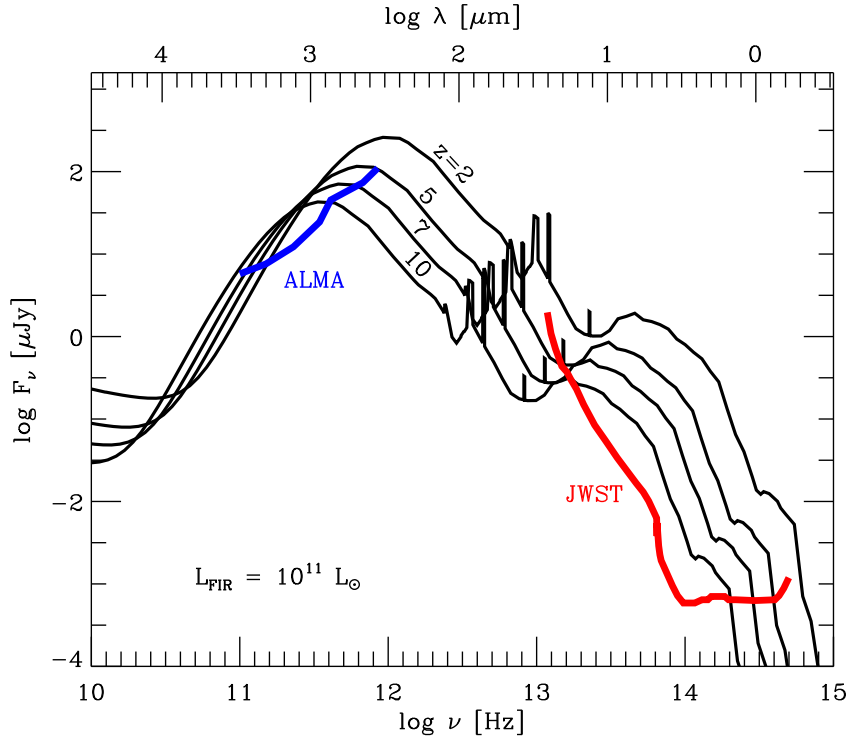


Fig. 5. Observed SED of a star forming galaxy with  $L_{\text{FIR}} = 10^{11} L_{\odot}$  (scaled from the SED of M82) at different redshifts ( $z=2, 5, 7$  and  $10$ , as labelled). Note that the observed flux at  $\lambda_{\text{obs}} \sim 1$  mm changes very little. The thick blue and red lines show the ALMA and JWST sensitivities for continuum detection at  $5\sigma$  with an integration of  $10^5$  sec.

by the cosmological dimming (Fig. 6), which makes any optical deep field dominated by galaxies at  $z < 1.5$ , and only a small fraction of galaxies at higher redshifts.

The negative K-correction allowed the discovery of a large number (a few 100) of starburst galaxies at high- $z$ , thanks to extensive surveys exploiting array of bolometers available on single dish telescopes (see e.g. Blain et al., 2002; Smail, 2006, for a review). Dusty starburst galaxies at high- $z$  discovered through the detection of their submm continuum are often dubbed as Sub-Millimeter Galaxies (SMGs). Although, high- $z$  dusty starbursts have been also discovered through observations in the mm band, for sake of simplicity we will refer to the whole population as “SMGs”.

Much effort has been invested for several years in the identification of the optical (or near-IR) counterparts of SMGs, mostly with the goal of determining their redshift through spectroscopic followup. However, as we will discuss in §3, the angular resolution of single dish telescopes is so low ( $11''$ – $18''$ ) that several optical/near-IR candidate counterparts are found within the telescope beam. The optimal way to identify the true counterpart would be to obtain mm-submm observations at higher angular resolution with a mm-submm in-

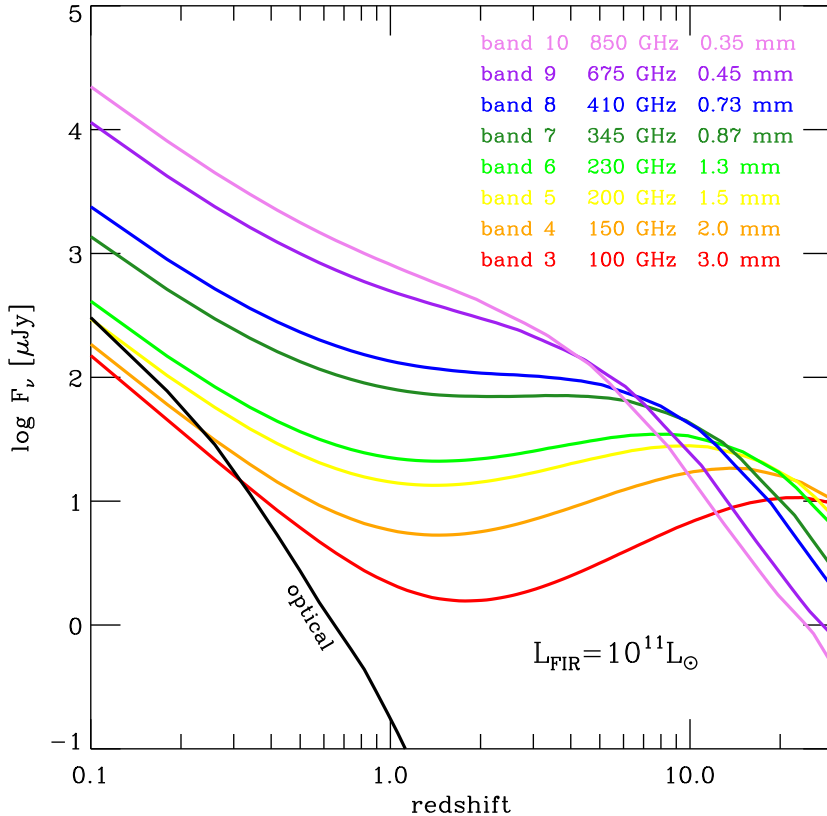


Fig. 6. Predicted flux densities of a star forming galaxy with  $L_{\text{FIR}} = 10^{11} L_{\odot}$  (by scaling the M82 template) observed in the different mm-submm ALMA bands. Note the nearly flat trend at  $1 < z < 10$  at wavelengths close to  $\sim 1$  mm. The predicted flux density in the optical ( $\lambda_{\text{obs}} = 5500 \text{ \AA}$ ) is also shown for comparison.

terferometer. However, as discussed in §3, the sensitivity to continuum of current mm-submm interferometers is low, making this approach very expensive in terms of observing time, especially if a statistically meaningful sample is needed.

Chapman et al. (2005) employed the alternative strategy of exploiting deep radio VLA observations. Given the tight correlation between far-IR thermal emission and radio synchrotron emission observed in galaxies, most SMGs should be associated with a detectable radio source. The higher angular resolution achievable with the VLA allowed Chapman et al. (2005) to locate the position of the SMGs with an accuracy high enough to position the slit for the spectroscopic identification. Note also that the large VLA primary beam, resulting into a large field of view, allowed the simultaneous radio detection of many SMGs in each single pointing. The identification of a prominent Ly $\alpha$  in many of the deep spectra provided the redshift for several tens SMGs. The SMGs redshift distribution resulting from these surveys is shown in Fig. 7

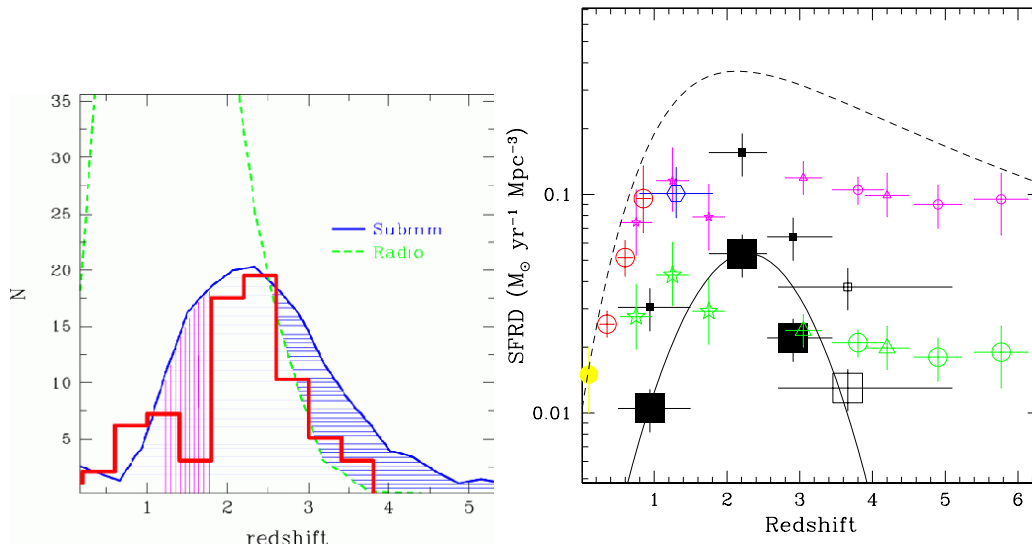


Fig. 7. *Left*: Redshift distribution of the SMG sample spectroscopically identified by Chapman et al. (2005) (red histogram). The blue line shows the model predicted redshift distribution, which may provide an indication on the redshift bias due to the radio selection criterion. *Right*: Contribution of SMGs (large squares) to the evolution of the density of star formation rate compared to estimates obtained by optical/UV surveys and radio/IR tracers (circles, triangles and stars). Small squares show a correction to the luminosity density of SMGs to account for the incompleteness due to the limiting flux of the redshift survey. See Chapman et al. (2005) for details.

(left), and it is characterized by a median redshift  $\langle z \rangle \sim 2.3$ . The redshift distribution is very similar to that of QSOs, suggesting a link between the two populations of objects.

The sample of SMGs for which a redshift has been measured is limited to a submm flux of a few mJy. The inferred redshifts imply far-IR luminosities of several times  $10^{12} L_{\odot}$ , i.e. extreme Ultra-Luminous Infrared Galaxies (more luminous, on average, than local ULIRG samples). Therefore, currently identified SMGs represent only the most luminous population of high- $z$  dusty starbursts (the tip of the iceberg). In Fig. 7 (right) the inferred contribution of SMGs to the density of star formation (SFRD) is compared with those inferred by UV/optical surveys and radio/IR tracers (Chapman et al., 2005). SMGs are indicated with large squares, while small squares show an attempt to account for the incompleteness due to the fact that current surveys only sample the most luminous sources, as discussed above. Clearly, once incompleteness is accounted for, SMGs contribute significantly to the history of star formation, especially at redshifts around two. Again, their evolution appears very similar to that of QSOs, suggesting a close link between SMGs and the evolution of massive halos which hosts QSOs.

The redshift determination of SMGs allowed also their millimetric spectroscopic followup with interferometers aimed at the detection of molecular transitions (which requires an accurate knowledge of the redshift due to the limited bandwidth). Intensive campaigns, especially with the IRAM PdB interferometer yielded the detection of CO rotational transitions for several SMGs (Greve et al., 2005), indicating that these galaxies also host huge amounts of molecular gas. The profile of the CO lines is often double-peaked, indicative of a rotating disk or of a merging of two galaxies. Followup interferometric observations at higher angular resolution have found that both the continuum and line emission are very compact in most SMGs, a few kpc or even less (Tacconi et al., 2006, 2008). The compactness of the SMGs provides constraints on the inferred central densities, which result much higher than in any other population of starburst galaxies, but comparable to those of compact passive galaxies found in the same redshift range. These findings, along with the huge inferred star formation rates, suggest that SMGs are progenitors of local massive ellipticals, experiencing their main episode of star formation, but which must undergo further structural evolution in order to reach the sizes observed in local ellipticals. These interferometric data also provide constraints on the global dynamical mass, typically yielding masses of a few times  $10^{11} M_{\odot}$  (e.g. Genzel et al., 2003, 2005). Interestingly, the inferred high density of massive galaxies ( $M > 10^{11} M_{\odot}$ ) at  $z \sim 2$  is difficult to reconcile with classical hierarchical models of galaxy evolution.

#### 2.4 Distant QSOs

Millimetric and submillimetric observations of distant AGNs are currently limited mostly to powerful QSOs (although we will later discuss the case of lower luminosity AGNs discovered in SMGs). Bolometric observations of large QSO samples have detected mm-submm continuum emission at the level of a few mJy in about 60 optically selected QSOs and about 20 radio galaxies at  $z > 1$ , out to  $z = 6.4$  (Omont et al., 2003; Carilli et al., 2001; Priddey et al., 2003; Isaak et al., 2002; Bertoldi et al., 2003a; Wang et al., 2008). Generally the detection rate achieved with current facilities is about 30% among bright QSOs. Detected QSOs have far-IR luminosities of about  $L_{\text{FIR}} \sim 10^{13} L_{\odot}$ , but these clearly represent the tip of the iceberg due to our current sensitivity limits.

For a fraction of high- $z$  QSO the inferred far-IR luminosity follows the same correlation with the radio luminosity as local star forming galaxies, suggesting that the far-IR luminosity is powered mostly by star formation (Wang et al., 2007). This result is supported by the Spitzer mid-IR detection, in a number of

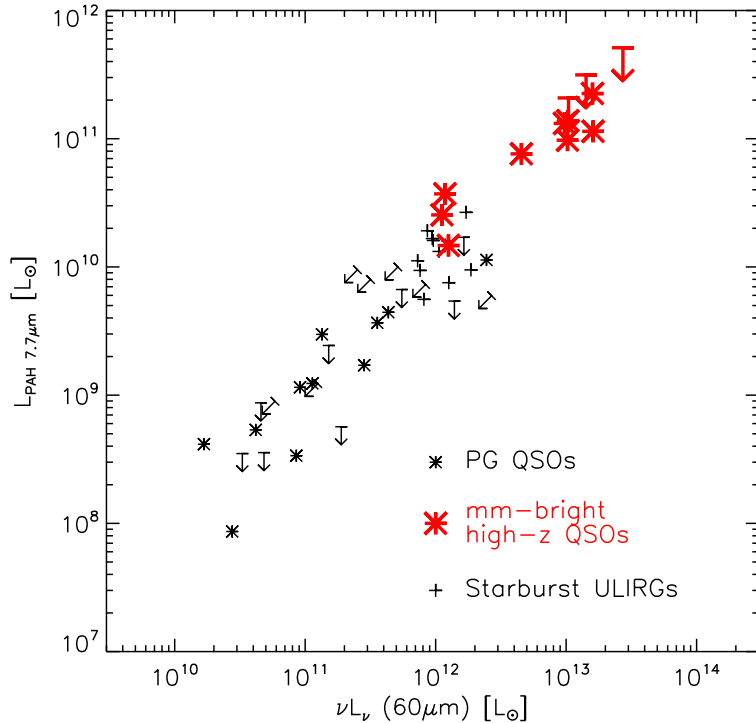


Fig. 8. Relationship between PAH  $7.7\mu\text{m}$  luminosity (which is a tracer of star formation) and far-IR luminosity (inferred from the mm/submm emission in high- $z$  QSOs). High- $z$  mm-bright QSOs follow the same relation of local starburst ULIRGs, indicating that the far-IR emission of the former is mostly due to star formation (from Lutz et al., 2008).

mm-bright QSOs, of strong PAH emission<sup>1</sup>, which is considered a good tracer of star formation (Lutz et al., 2007, 2008). Moreover, the PAH luminosity is found to correlate with the far-IR luminosity and following the same relation of starburst galaxies (Fig.8), further supporting the starburst origin of the far-IR emission.

The star formation rates inferred from the far-IR luminosity (as well as from the PAH luminosity) are as high as a few times  $1000 M_{\odot} \text{ yr}^{-1}$ . This suggests that in mm-bright QSO we are witnessing the simultaneous growth of black holes (as traced by the optical and X-ray AGN emission) and of the stellar mass in their host galaxy (as traced by the far-IR), which will probably evolve into massive ellipticals (Granato et al., 2004; Di Matteo et al., 2005). Such a co-coeval growth is expected in models of BH-galaxy evolution aimed at explaining the local relation between spheroids and BH mass (Ferrarese & Merritt, 2000; Gebhardt et al., 2000; Marconi & Hunt, 2003).

<sup>1</sup> The Polycyclic Aromatic Hydrocarbon (PAH) molecules are macro-molecules, or very small dust grains, which are excited by the (soft) UV radiation field in star forming regions and emit strong features mostly at  $6\text{--}11\mu\text{m}$ . These species are mostly destroyed in the strong radiation field produced by AGNs.

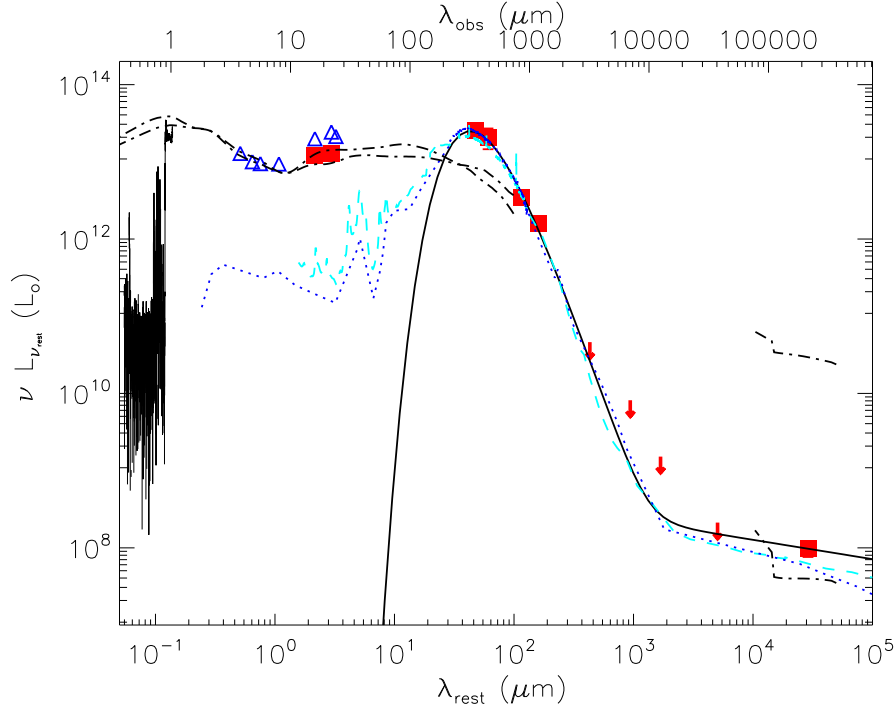


Fig. 9. Near-IR to radio spectral energy distribution of one of the most distant QSOs, J1148+5152, at  $z=6.4$ . Red and blue points show the observed photometry, while curved lines show a combination of QSO and starburst templates fitting the data. Note the prominent thermal far-IR emission, indicative of a large amount of dust (a few times  $10^8 M_\odot$ ) already present in this object close to the epoch of re-ionization. Adapted from Beelen et al. (2006).

However, the relation between star formation and black hole accretion (i.e. the relation between  $L_{\text{FIR}}$  and  $L_{\text{opt}}$ ) seems to saturate at high luminosities (Lutz et al., 2008; Maiolino et al., 2007a), suggesting that at high- $z$  the BH growth proceeds more rapidly than the host growth.

The high far-IR luminosities inferred from the mm-submm observations also imply large amount of dust in the host of high- $z$  QSOs. Accurate measurements of the dust mass are however difficult to obtain due to the unknown dust temperature and emissivity. Multiple band observations greatly help to remove the degeneracy between these quantities (Beelen et al., 2006; Wang et al., 2007). Fig.9 shows the rest-frame infrared SED of one of the most distant QSOs ( $z=6.4$ ) known so far, for which the far-IR thermal bump is relatively well sampled thanks to various submm and mm observations. The inferred dust masses are as high as several times  $10^8 M_\odot$ . The discovery of such huge masses of dust in the most distant QSOs is puzzling. Indeed, in the local universe the main source of dust are the atmospheres of evolved stars (mostly AGB). However, at  $z>6$  the age of the Universe is less than 1 Gyr, which is the minimum time required for AGB stars to evolve in large numbers and to significantly enrich the ISM with dust. This suggests that in the early universe other mechanisms dominate the dust production. Core-collapse SNe are candidate sources

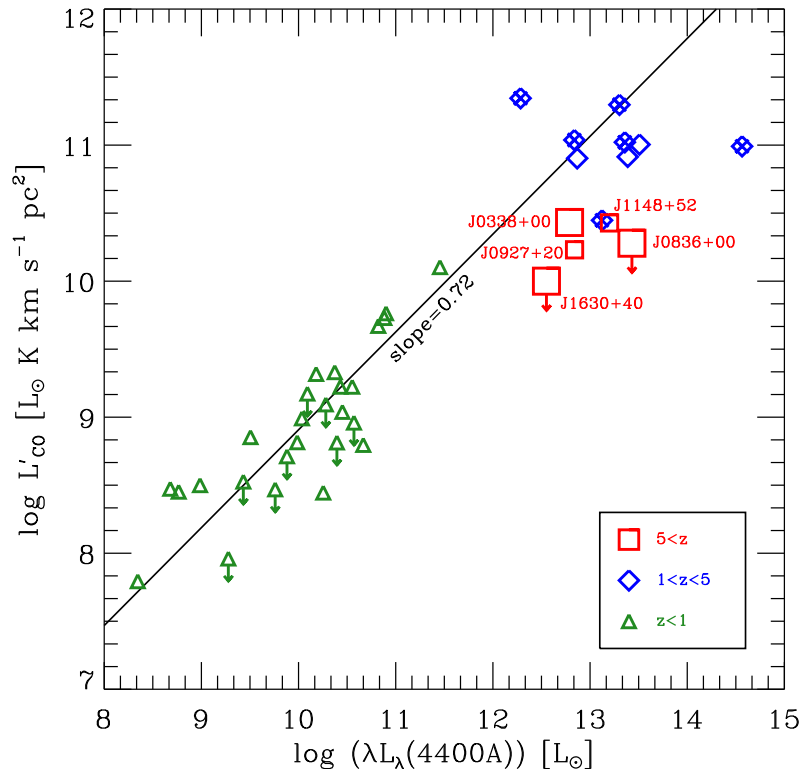


Fig. 10. Correlation between the CO luminosity (tracing the molecular gas mass) and optical luminosity of QSOs (tracing the black hole accretion rate). Note the non-linear relation between the two quantities. From Maiolino et al. (2007b).

of dust on short timescales. Observations have indeed found dust formed in SN ejecta (Sugerman et al., 2006; Rho et al., 2008), as also expected on theoretical grounds (Todini & Ferrara, 2001; Nozawa et al., 2003). The extinction curve inferred in high- $z$  QSOs and galaxies appears in agreement with that expected for dust produced in SN ejecta (Maiolino et al., 2004; Stratta et al., 2007; Willott et al., 2007), supporting the idea that SNe may indeed be the major source of dust in the early universe. However, even with the highest dust yield observed so far, the huge mass of dust inferred from mm-submm observations of the most distant QSOs remains difficult to account for (Dwek et al., 2007).

Extensive reviews on the CO emission in high- $z$  objects, and in AGNs in particular, are given in Solomon & Vanden Bout (2005) and in Omont (2007). More than half of the  $\sim 40$  CO detections obtained at high redshift ( $z > 1$ ) are in AGNs (QSOs or radio galaxies). In particular, all of the detections at  $z > 3.5$  are in AGNs. The higher detection rate in high- $z$  QSOs is mostly due to their huge far-IR luminosities and to the CO-FIR correlation (§2.1). The molecular gas masses inferred from the CO detections are of the order of a few times  $10^{10} M_{\odot}$ . Except for the huge amounts of molecular gas, the general properties



of the CO emission in high- $z$  QSOs and radio-galaxies do not differ strongly from local and lower redshift powerful starbursts. The observation of multiple CO transitions suggests that the CO excitation temperature is higher in some QSOs (e.g. Weiß et al., 2007), but the statistics are still very low. The CO emission follows the same trend with the FIR luminosity observed in Fig. 3, indicating that QSO host galaxies are experiencing a strong starburst event in the process of rapidly exhausting the available molecular gas, on a time scale of only  $\sim 10^7$  yrs. It is interesting to note that the relation between CO luminosity (tracing the amount of molecular gas) and optical luminosity (tracing the black hole accretion rate in QSOs) is not linear, as shown in Fig. 10 (Maiolino et al., 2007b). This result indicates that, while the black hole can accrete at very high rates (limited only by its Eddington luminosity), the host galaxy has only a limited amount of molecular gas available for star formation (given by the galaxy evolutionary mechanism); hence the two formation processes probably occur on different time scales (as already discussed above).

Deep observations have allowed the detection of transitions from other molecular and atomic species, such as HCN, HCO<sup>+</sup>, HNC, CN and CI, which are tracers of high density gas and of the gas chemistry and excitation (e.g. Carilli et al., 2005; Wagg et al., 2005; Riechers et al., 2006; García-Burillo et al., 2006; Guélin et al., 2007; Weiß et al., 2005a). However, these detections are limited to very few bright sources, due to the limited sensitivity of current facilities. Within the limited statistics available, the intensity of these lines relative to CO and to  $L_{\text{FIR}}$  do not differ strongly from lower redshift and local starburst galaxies (although there are indications that the intensity of HCN decreases at high luminosities; Gao et al., 2007; Riechers et al., 2007).

Recently, deep observations achieved the first detection of the [CII] fine structure line at  $158\mu\text{m}$  in two high- $z$  QSOs (Fig. 11) (Maiolino et al., 2005; Iono et al., 2006). This line is emitted by Photo-Dissociation Regions (PDRs) in star forming galaxies, and it is the strongest line in the spectrum of nearly any galaxy. The ratio  $L_{\text{[CII]}}/L_{\text{FIR}}$  observed in these two high- $z$  QSOs is about  $2 - 4 \cdot 10^{-4}$ , i.e. similar to the value observed in local ULIRGs. The detection of [CII] with a luminosity relative to  $L_{\text{FIR}}$  similar to local sources suggests that these high- $z$  systems have already been enriched with heavy elements, and with carbon in particular (Maiolino et al., 2005).

Generally the angular resolution and sensitivity are not good enough to trace CO rotational curves and therefore to obtain accurate constraints on the dynamical mass. However, in some high- $z$  bright AGN the kinematics is resolved, especially in lensed cases, where the lensing shear helps to resolve the galaxy structures (e.g. Kneib et al., 1998; Venturini & Solomon, 2003; Lewis et al., 2002; Omont et al., 1996; De Breuck et al., 2005; Papadopoulos et al., 2000). In other unresolved, or marginally resolved QSOs the width of the CO line, along with measurements (or limits) on the size of the CO emitting region

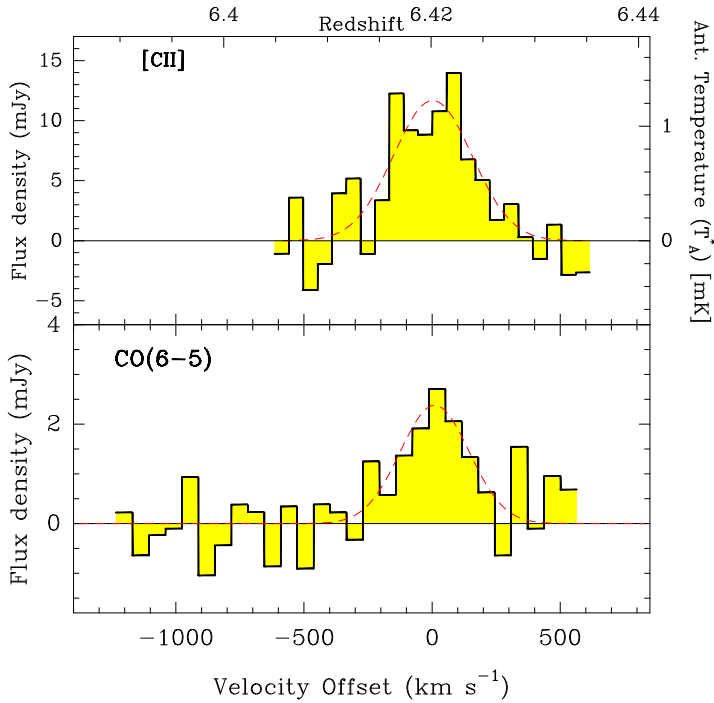


Fig. 11. *Upper panel:* Detection of the [CII]158 $\mu$ m fine structure line in one of the most distant quasars known, J1148+5152, at  $z=6.4$  (Maiolino et al., 2005). *Lower panel:* The CO(6–5) transition observed in the same objects is shown for comparison (Bertoldi et al., 2003b; Walter et al., 2003). Note the different flux scales on the two panels.

provide some constraints on the dynamical mass (e.g Maiolino et al., 2007b). Typical dynamical masses inferred for QSO hosts and radio galaxies are of the order of a few times  $10^{11} M_{\odot}$ . However, we should recall that current observations sample only the “tip of the iceberg” of the AGN population at high redshift.

Recently, Ho (2007) attempted to calibrate the width of CO lines in galaxies as a proxy of their dynamical masses. Once this calibration is applied to the host of QSOs, the resulting galaxy mass can be compared with the black hole mass inferred from their optical-UV emission lines. An interesting result is that high- $z$  QSOs appear to deviate from the local BH-galaxy mass relation, in the sense that their hosts are less massive than expected. This result is in agreement with other independent indications that the BH-galaxy mass relation evolves at high redshift (Peng et al., 2006; McLure et al., 2006). However, one should be careful when using the CO line width as a tracer of the dynamical mass in (unobscured) QSOs. Indeed, selection effects make QSOs hosts to be viewed preferentially face-on, since edge-on views tend to be obscured. As a consequence, the observed width of the CO line in QSOs is likely reduced due to projection effects (Carilli & Wang, 2006), and may not be representative of the intrinsic rotation of the CO disk (Wu, 2007).

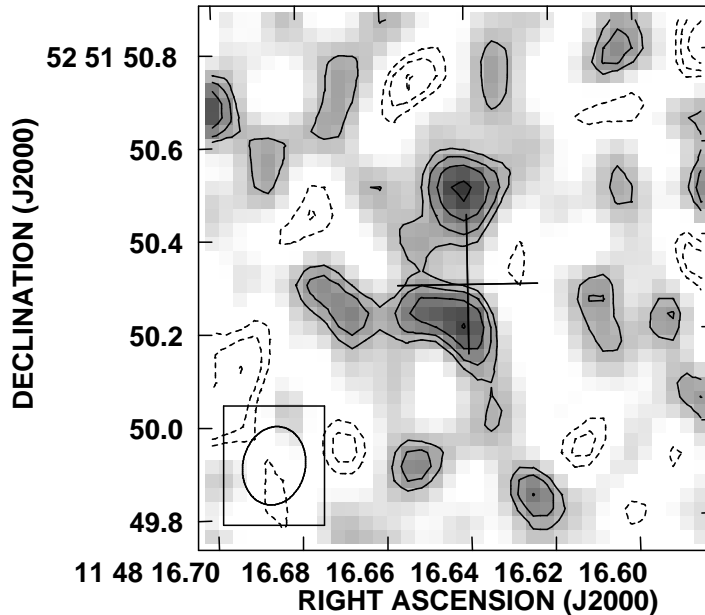


Fig. 12. CO(3–2) map of the central region of J1148+5152, a QSO at  $z=6.4$  (from Walter et al., 2004). At this redshift the angular resolution of  $\sim 0.15''$  corresponds to about 800 pc.

An interesting particular result is the CO(3–2) map of one of the most distant QSOs, J1148+5152, at  $z=6.4$  (Fig. 12) (Walter et al., 2004). The map shows resolved emission extending over about 5 kpc and two central peaks separated by 1.7 kpc. From the velocity structure Walter et al. (2004) infer a dynamical mass of about  $5 \cdot 10^{10} M_{\odot}$ . This mass is much lower than the mass of a few times  $10^{12} M_{\odot}$  that would be expected from the black hole mass derived for the same object (a few times  $10^9 M_{\odot}$ ) if applying the local BH-bulge mass relation. This result would provide further support to the scenario where at high- $z$  black holes grow faster than their host galaxies, while the latter reach the local BH-bulge relation only at lower redshifts. However, observations at higher angular resolution and with higher sensitivity are certainly required to better determine the dynamical mass, and remove the degeneracy with the inclination angle of the putative disk.

Above we have discussed mm-submm observations aimed at specifically investigating objects known to host powerful AGNs (QSOs or radio-galaxies). We can however consider the orthogonal approach: do galaxies discovered at mm-submm wavelengths (SMGs) host AGNs? This issue has been investigated with the aid of deep X-ray observations. Alexander et al. (2003, 2005) found that most SMGs do host a X-ray source whose luminosity and spectral shape can only be ascribed to the presence of an obscured AGN. However, even when corrected for absorption, the inferred AGN luminosity cannot account for far-IR luminosity observed in SMGs, hence the main source of far-IR emission in SMGs is due to star formation. Similar results were obtained

more recently thanks to Spitzer mid-IR spectroscopy (Valiante et al., 2007; Menéndez-Delmestre et al., 2007; Pope et al., 2008). The detection of strong PAHs in the spectra of most SMGs supports the scenario where most of the luminosity is due to star formation. The detection of a weak mid-IR continuum due to hot dust does trace the presence of an obscured AGN in some SMGs, but with a bolometric power much lower than the starburst component. Summarizing, SMGs represent a critical phase in the formation of massive galaxies; black hole accretion is accompanying this major star formation event, but at a rate much lower than observed in QSOs.

### 3 Current mm-submm facilities

Millimetric and submillimetric facilities can be divided in two main classes: single dish telescopes and interferometers. These two classes of facilities are often complementary, especially in extragalactic astronomy, one generally being characterized by wider field of view and higher sensitivity to continuum, the other providing higher angular resolution and higher sensitivity for line detection. This section provides a short overview of the current facilities in both classes, by also discussing their main relative advantages and limitations.

#### 3.1 *Single dish telescopes*

A list of the main currently available single dish mm-submm telescopes is given in Tab. 1. Current single dish telescopes have a diffraction-limited angular resolution of only about 10–20". However, one of the main advantages of single dish telescopes relative to interferometers is their wide field of view, which makes single dish telescopes optimally suited for wide area surveys. All single dish telescopes are equipped with various heterodyne receivers for spectroscopy. However, an additional advantage of single dish telescopes is the possibility of using bolometers, which (thanks to their wider band width) are more sensitive to the continuum emission than heterodyne receivers. To fully exploit the large field of view for the detection of mm-submm sources, observatories have developed cameras hosting large bolometer arrays that allow the simultaneous observation of wide areas of the sky. Tab. 1 lists the main bolometer cameras currently available, with a short summary of their characteristics (number of detectors, wavelength of operation, field of view). Most of the high redshift submillimeter galaxies known so far have been discovered thanks to such bolometer arrays. Some of these single dish observatories are dedicating an increasing fraction of their total observing time to extensive surveys by exploiting these bolometer cameras. Probably this will be one of the main working modes for some single dish telescopes when ALMA will be in

Table 1  
Main mm-submm single dish telescopes currently available

Name	Diam. [m]	$\Delta\lambda^a$ [mm]	Beam ( $\lambda$ ) <sup>b</sup> [arcsec] ([mm])	Bolometer arrays			
				Name	$N_{det}^c$	$\lambda^d$ [mm]	FOV <sup>e</sup> [arcmin <sup>2</sup> ]
IRAM	30	1.2–3	11 (1.2)	MAMBO	117	1.2	3 <sup>f</sup>
JCMT	15	0.45–1.2	15 (0.87)	SCUBA-2 <sup>g</sup>	10 <sup>4</sup>	0.45–0.87	55
CSO	10.4	0.35–1.2	9 (0.35)	SHARC-II	384	0.35–0.85	2.6
				Bolocam	115	1.1–2.1	50 <sup>f</sup>
APEX	12	0.20–1.2	19 (0.87)	LABOCA	295	0.87	102 <sup>f</sup>
				SABOCA <sup>g</sup>	37	0.35	1.1 <sup>f</sup>
ASTE	10	0.35–0.87	17 (0.87)			–	
Nobeyama	45	3.4–10	15 (3)			–	
LMT <sup>h</sup>	50	0.85–4	7 (1.2)	AzTeC <sup>i</sup>	144	1.1–2.1	2.4 <sup>f</sup>

Notes:

<sup>a</sup> Wavelength range of operations (in units of mm).

<sup>b</sup> Beam size (FWHM), in arcsec, at the wavelength given in parenthesis (in mm).

<sup>c</sup> Number of detectors in the array.

<sup>d</sup> Wavelength(s) of operations (in mm).

<sup>e</sup> Field of view of the array in arcmin<sup>2</sup>.

<sup>f</sup> In these arrays the quoted FOV is not filled with detectors, and the effective FOV (i.e. the region of the sky instantaneously sampled in one single pointing) may be lower even by a factor of  $\sim 4$ .

<sup>g</sup> Under commissioning at the time of writing.

<sup>h</sup> Under construction at the time of writing.

<sup>i</sup> While awaiting for LMT, AzTeC has already been successfully used at JCMT and ASTE.

operation: single dish telescopes will provide continuum targets through wide area surveys to be then observed in depth with ALMA (to obtain spectroscopic information, multi-band data, and angular resolution information).

It is worth noting that some of these single dish telescopes are also being equipped with very broad band heterodyne receivers, which will allow astronomers to identify the redshift of high- $z$  sources through the detection of multiple CO transitions (these instruments are often dubbed “redshift machines”, Erickson et al., 2007; Glenn et al., 2007; Stacey et al., 2007; Harris et al., 2007)

However, one of the main problems of single dish telescopes in extragalactic astronomy is their limited capability of detecting broad faint emission lines, as

Table 2

Main mm-submm interferometers currently available

Name	Antennas	$\Delta\lambda$	Max ang. resol.	Total area
	[# $\times$ Diameter]	[mm]	[asec]	[m <sup>2</sup> ]
IRAM-PdBI	6 $\times$ 15m	1.2–3	0.35	1060
CARMA <sup>a</sup>	6 $\times$ 10.4m + 10 $\times$ 6m	1.2–3	0.1	792
NMA	6 $\times$ 10m	1.2–3	1	471
SMA	8 $\times$ 6m	0.35–1.2	0.1	226
eSMA <sup>b</sup>	SMA + 15m + 10.4m	0.87–1.2	0.2	488
ATCA <sup>c</sup>	6 $\times$ 22m <sup>d</sup>	3–12	2.	2280 <sup>d</sup>

Notes:

<sup>a</sup> CARMA is the merging of the former OVRO (6 $\times$ 10.4m antennas) and BIMA (10 $\times$ 6m antennas) arrays.

<sup>b</sup> eSMA is the combination of SMA with the JCMT and CSO.

<sup>c</sup> ATCA can observe at much lower frequencies, down to  $\lambda = 20$ cm, the specifications given here only refer to the observing capabilities at mm wavelengths.

<sup>d</sup> At  $\lambda = 3$ mm only 5 of the ATCA antennas can be used, for a total collecting area of 1900 m<sup>2</sup>.

a consequence of the (pseudo-continuum) baseline variability. Although various techniques are employed to subtract the background emission (position switching, beam switching, frequency switching), the background variability is often so rapid and irregular that the resulting spectrum is affected by a residual pseudo-continuum, generally tilted or curved. Such underlying curved baseline is generally not much of a trouble for Galactic studies, where emission lines are very narrow (hence the underlying baseline can be easily fitted and subtracted). However, this is one of the main concerns for studies of faint objects in extragalactic studies, where lines are relatively broad (a few 100 km/s) and may be confused or washed out by curved baselines.

### 3.2 Interferometers

Interferometers have obviously the advantage of much higher angular resolution relative to single dish telescopes. Depending on their configuration and on the specific facility, current interferometers yield beam sizes ranging from a few arcsec to a few tenths of arcsec. Needless to say that the most detailed maps of millimeter lines have been obtained with interferometers, both in local galaxies and in distant systems.

Even when distant galaxies are not resolved, interferometers remain the best tools to detect faint emission lines. The issue of artificially curved/tilted base-

lines does not apply to interferometers, since the source used for phase reference also calibrates and removes the variations in sky transmission/emission. As a consequence, faint emission lines in distant galaxies were mostly detected with interferometers.

While superior for spectroscopy and line detection, interferometers have suffered limited sensitivity to continuum emission. Indeed, until recently, interferometers have been equipped with relatively narrow band receivers ( $\Delta\nu \sim 500$  MHz). Since the continuum sensitivity scales as  $(\Delta\nu)^{1/2}$ , this has made interferometers not competitive for continuum detection relative to bolometers on single dish telescopes (whose band width is generally limited by the adopted filters,  $\Delta\nu \sim 50$  GHz). However, more recently some interferometers have been equipped with wider band receivers (e.g. the new IRAM-PdBI receivers with  $\Delta\nu \sim 4$  GHz) therefore greatly improving their sensitivity to continuum.

Tab. 2 lists the main mm-submm interferometers currently available. The IRAM array (located on the Plateau de Bure, French Alps) is the one with the largest collecting area, and the most sensitive in the 1–3 mm range. CARMA (located on Cedar Flat, California) is the recent merging of the former BIMA and OVRO arrays; even with the combination of these antennas CARMA does not reach the same collecting area of IRAM, but is expected to achieve higher angular resolution ( $\sim 0.1''$ ). SMA (located on Mauna Kea, Hawaii) is the only array working at submm wavelengths, down to  $350\mu\text{m}$ . It can also work in combination with the JCMT and CSO (Tab. 1); this configuration, dubbed as “extended-SMA” or “eSMA”, doubles the total collecting area of the SMA, but it is limited to  $\lambda > 870\mu\text{m}$ .

## 4 ALMA

The “Atacama Large Millimeter Array”, ALMA, will provide a jump of nearly two orders of magnitude in sensitivity and angular resolution with respect to existing facilities. It is therefore expected to provide major step forwards and breakthroughs in many fields of astronomy. Some specific key scientific cases, which drove the ALMA design, are: 1) The ability to detect spectral line emission from CO or C<sup>+</sup> in normal galaxies (Milky Way-like) at  $z \sim 3$  in less than 24 hours of observation. 2) The ability to image the gas kinematics in protostars and protoplanetary disks around young Sun-like stars at a distance of 150 pc (i.e. roughly the distance of the star forming regions in Ophiuchus or Corona Australis), enabling one to study their physical, chemical and magnetic field structures and to detect the tidal gaps created by planets undergoing formation in the disks. 3) The ability to provide high quality images at an angular resolution of at least  $0.1''$ . The achievement of these scientific goals require: a) an array of antennas; b) submm capabilities; c) a collecting area  $> 6000 m^2$ ;

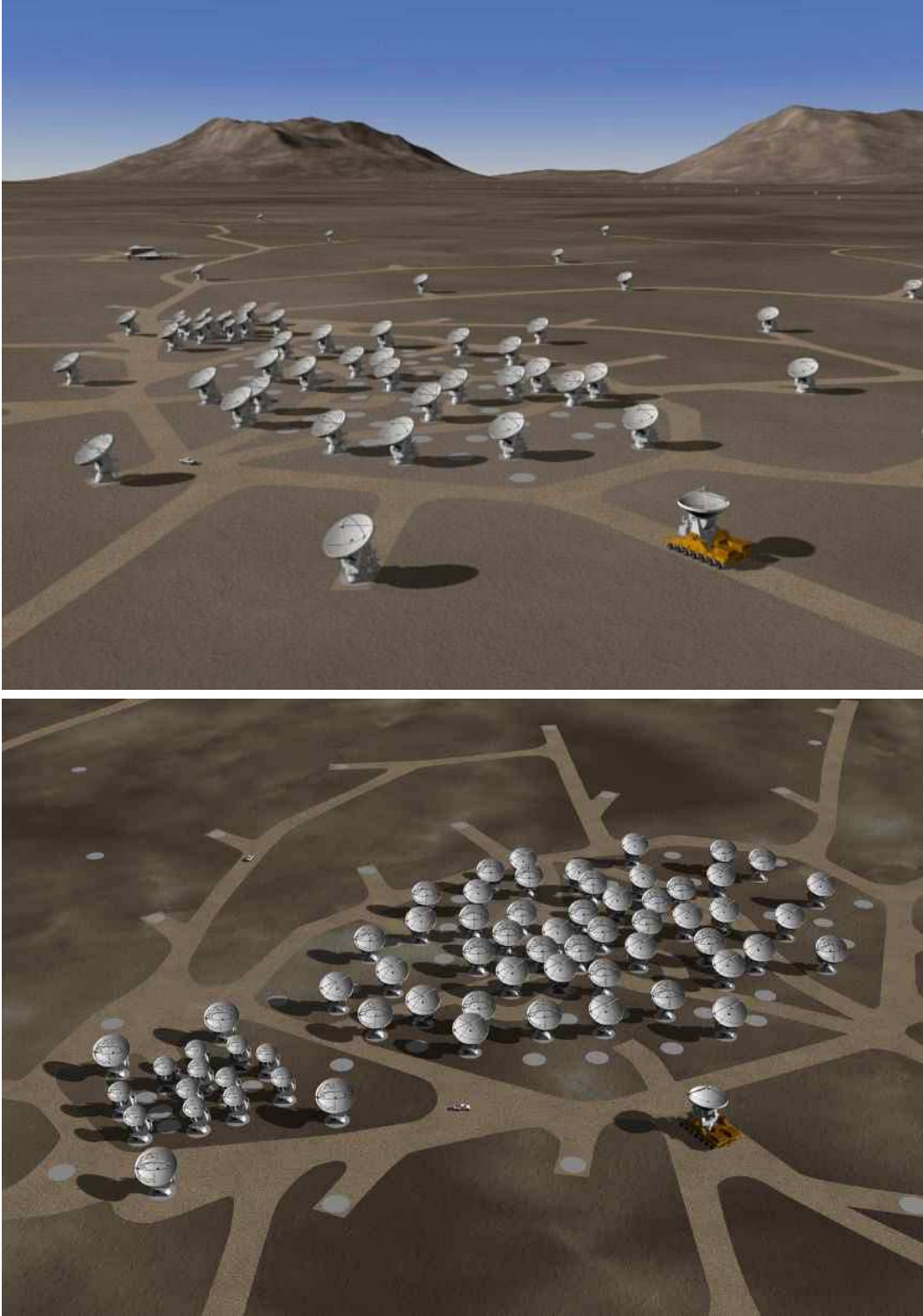


Fig. 13. *Top*: Artistic view of the ALMA array on Chajnantor Plateau, in an extended configuration. *Bottom*: Close up of the ALMA array in its compact configuration, showing more clearly also the Atacama Compact Array (ACA), located in the bottom-left region. The antenna transporter is also illustrated in operation in both panels (bottom-right). Courtesy of the European Southern Observatory.



d) a site which is high, dry, large and flat. These are the considerations that mostly drove the design and development of ALMA.

The magnitude of the project is so large, both in terms of required funding and in terms of technical developments, that it necessarily needs the joint contribution of various international institutes and agencies. ALMA is now a world-wide project involving Europe (through the European Southern Observatory, ESO), North America (U.S.A and Canada, through the National Radio Astronomical Observatory, NRAO), East Asia (Japan and Taiwan, through the National Astronomical Observatory of Japan, NAOJ), and the host country Chile. Detailed information on the project can be found at the web sites of these agencies (e.g. <http://www.eso.org/projects/alma/>, <http://www.alma.nrao.edu/>, <http://www.nro.nao.ac.jp/alma/E/>, <http://www.alma.cl/>). In the following I will only summarize the main technical features of ALMA and its main observing capabilities.

ALMA consists of at least  $54 \times 12\text{m}$  antennas and  $12 \times 7\text{m}$  antennas for a total collecting area of at least  $6500 \text{ m}^2$ . The antenna configurations will cover baselines ranging from 200 m out to 18 km, yielding a maximum angular resolution better than  $0.1''$  at 3mm, and better than  $0.01''$  at submm wavelengths (Tab. 3). The field of view is limited by the primary beam of individual antennas and it ranges from  $1'$  at 3mm to about  $10''$  at submm wavelengths (Tab. 3). Fig. 13 shows an artistic view of the ALMA array in extended and compact configurations. The 7m antennas and 4 of the 12m antennas are clustered into the 'Atacama Compact Array', ACA (Fig. 13), which will have a compact fixed configuration aimed at covering the  $uv$  plane on short spacings. ACA will be crucial to recover diffuse emission extending on scales larger than a few arcsec (which is resolved out by the ALMA array).

ALMA will be located on Chajnantor Plateau, in the Atacama desert (Chile), at an altitude of 5000 m. This is an exceptionally dry site providing a good transparency even in the  $350\mu\text{m}$  and  $450\mu\text{m}$  windows for a significant fraction of the time. In particular, the Precipitable Water Vapor (the main source of opacity) is  $\text{PWV} < 1 \text{ mm}$  for more than 50% of the time, at least during the winter months (Fig. 14). The vast flat topography of Chajnantor Plateau is optimal to accommodate the various array configurations, providing some constraints on the location of the antennas only in the most extended configuration. The antennas will be moved from one station to the other by means of huge trucks at a rate of 2 antennas/day.

As listed in Tab. 3, receivers for 6 frequency bands are currently fully funded (bands 3, 4 and 6–9). Band 5 (163–211 GHz) is currently planned only for 6 antennas. The funding and the specifications of band 10 are pending, since the receivers development is still in progress. The distribution of the ALMA bands relative to the atmospheric windows is illustrated in Fig. 1. The maxi-

Table 3  
 Frequency bands currently planned for ALMA

Band	$\Delta\nu$	$\Delta\lambda$	ang. res. <sup>a</sup>	FOV <sup>b</sup>	cont. sens. <sup>c</sup>	line sens. <sup>d</sup>
	[GHz]	[mm]	[arcsec]	[arcsec]	[mJy]	[mJy]
3	84–116	2.6–3.6	3.0–0.034	56	0.05	0.42
4	125–169	1.8–2.4	2.1–0.023	48	0.06	0.45
5 <sup>e</sup>	163–211	1.4–1.8	1.6–0.018	35	0.77	6.8
6	211–275	1.1–1.4	1.3–0.014	27	0.10	0.58
7	275–373	0.8–1.1	1.0–0.011	18	0.20	0.96
8	385–500	0.6–0.8	0.7–0.008	12	0.37	1.6
9	602–720	0.4–0.5	0.5–0.005	9	0.60	2.1
10 <sup>f</sup>	787–950	0.3–0.4	0.4–0.004	7	0.90	2.7

Notes:

<sup>a</sup> Angular resolution in arcsec in the compact (200 m) and in the most extended configuration (18 km).

<sup>b</sup> Field of view in arcsec estimated as the Full Width Half Maximum of the primary beam.

<sup>c</sup> Continuum sensitivity: rms (in mJy) in one minute of integration, derived by using the ESO ETC. The weather conditions were automatically selected by the ETC depending on the band.

<sup>d</sup> Emission line sensitivity: rms (in mJy) in one minute of integration, derived by using the ESO ETC and by assuming a line width of 300 km/s.

<sup>e</sup> Initially only 6 antennas will be equipped with band 5 (which explains the much lower sensitivity in this band).

<sup>f</sup> Funding of band 10 is still pending, awaiting results from the technical development. The sensitivity and frequency range quoted for this band are just indicative, and may be subject to significant variations depending on technical constraints.

mum simultaneous frequency coverage allowed by the huge correlator is 8 GHz, which allows ALMA to reach high sensitivities even for the continuum detection. Tab. 3 summarizes the ALMA sensitivities (both for continuum and line detection). For instance, in band 7 (870 $\mu$ m) ALMA reaches the extraordinary sensitivity of  $\sim 0.1$  mJy (rms) in one minute of integration, to be compared with the SCUBA sensitivity of about 1 mJy (rms) in 1 hour of integration.

Constructions at the ALMA site started already a few years ago and are now nearly completed. At the time of writing the first eight antennas have arrived for integration and testing at the Operations Support Facilities (OSF, located at about 30 km from the ALMA site). In early 2009 the first three antennas will be moved to the ALMA Operations Site (AOS) for commissioning. In 2010 a call for proposal is planned for early science with an initial set of at least 16 antennas. The full array is scheduled to come in full operation in 2012.

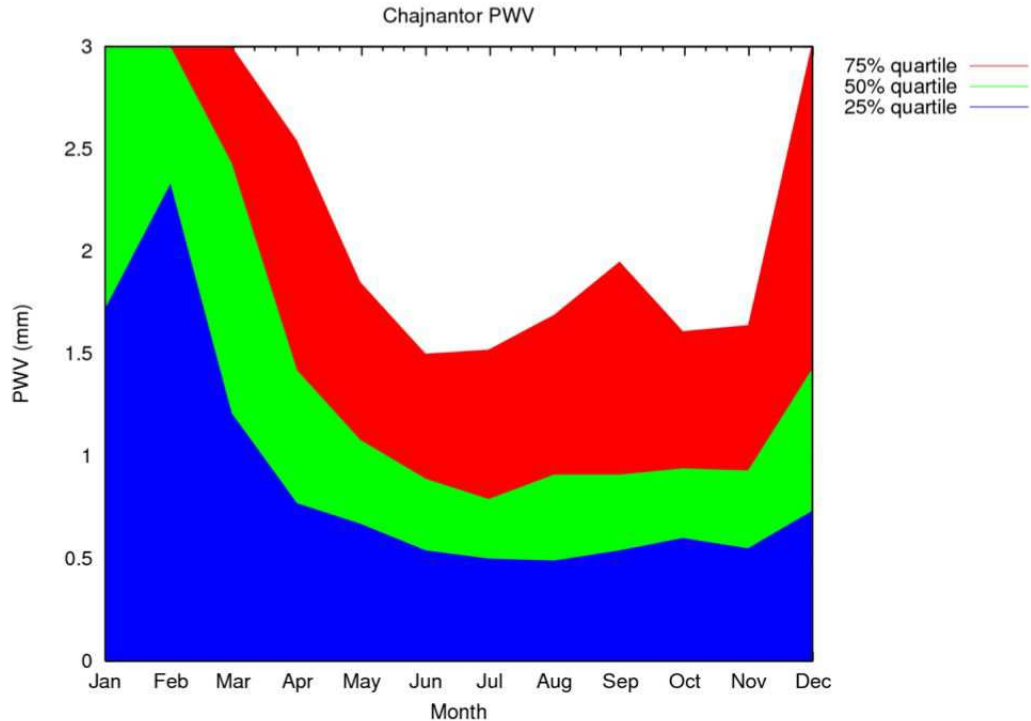


Fig. 14. Statistics of the Precipitable Water Vapor (the main source of opacity at mm-submm wavelengths) during the year at Chajnantor Plateau. Note that during the winter months  $PWV < 1$  mm for more than 50% of the time, allowing very sensitive observations at submm wavelengths. Courtesy of the European Southern Observatory.

An important feature of the ALMA organization is the plan of making it an observing facility easily accessible also by non-experts in the field. Both the software to prepare the observations and the pipeline for the data reduction are designed to be easy to use also by people that are not necessarily experts in interferometry nor necessarily acquainted with mm/submm observing techniques. This is an important characteristic that will make ALMA totally open to a broad astronomical community.

## 5 ALMA prospects for AGN studies

It is obvious that the ALMA capabilities will allow astronomers to tackle numerous outstanding issues, spanning most of the research fields in astronomy. A summary of some of the main scientific goals can be found in the Design Reference Science Plan (DRSP), available at <http://www.strw.leidenuniv.nl/alma/drsp11.shtml>. It is beyond the scope of these lecture notes to provide an overview of the several outstanding scientific cases for ALMA. In this section I will only focus on some of the ALMA prospects for AGN studies and some related topics, but

even in this field the discussion is not meant to be exhaustive.

### 5.1 Local AGNs

One of the most hotly debated issues on AGNs is the physics, structure and dynamics of the circumnuclear molecular medium, which is both responsible for the obscuration of AGNs and presumably related to their feeding. Some models assume a uniform gas distribution in a toroidal geometry, whose thickness is supported by IR radiation pressure (e.g. Krolik, 2007). Other models propose that the circumnuclear obscuring medium is clumpy and originated by the outflow of the accretion disk (Elitzur & Shlosman, 2006; Nenkova et al., 2002; Hönig et al., 2006). Yet other models assume a clumpy distribution due to the effects of supernova explosions or stellar winds, which are also responsible for making the medium “thick” (Wada & Tomisaka, 2005; Watabe & Umemura, 2005; Nayakshin & Cuadra, 2007). The high angular resolution, along with its spectroscopic capabilities, will allow ALMA to clearly distinguish between these models, both through morphological analyses and by investigating the kinematics of the nuclear and circumnuclear medium. Fig. 15 shows the expected distribution of circumnuclear CO emission according to the torus model in Wada & Tomisaka (2005), and convolved with the angular resolution of ALMA projected at the distance of NGC 1068 (panel *c*): the clumpy nature of the “torus” is clearly resolved.

Actually, the structure shown in Fig. 15 describes the extended component of the torus (radius  $\sim 32$  pc), which contains a large amount of gas, but accounts only for a small fraction of the nuclear obscuration. Most of the obscuration is due to dense gas on the parsec scale (Maiolino & Risaliti, 2007), as also inferred by mid-IR interferometric observations (Jaffe et al., 2004). In clumpy models the dust within each individual cloud spans a wide range of temperatures and therefore emits strongly at all wavelengths, from mid-IR to submm. As a consequence, an interesting prediction of clumpy models is that the nuclear “torus”, made of out of several clouds, should show the same morphology at all infrared wavelengths<sup>2</sup>. In contrast, uniform “torus” models expect a strong radial temperature gradient and, therefore, the innermost warm dust should emit much more at mid-IR wavelengths, while submm radiation from cold dust should be observed mostly in the outer regions. At high frequencies ALMA has an angular resolution matching VLTI (i.e. sub-pc scale at the distance of famous AGNs such as NGC 1068 and Circinus), therefore it will be possible to directly compare the mid-IR morphology with the submm morphology and directly test the predictions of clumpy and uniform torus

---

<sup>2</sup> Actually some difference of the morphology as a function of wavelength is expected, but well predicted by models.

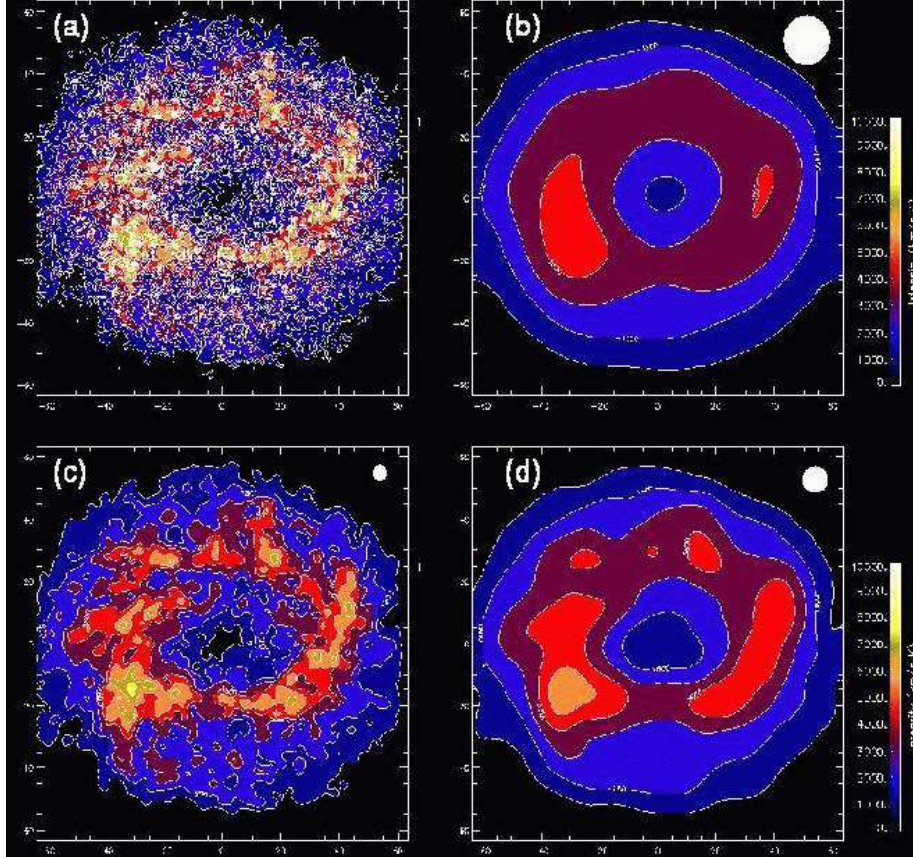


Fig. 15. CO(2–1) intensity map of NGC 1068 resulting from the extended torus AGN model in Wada & Tomisaka (2005). The top-left panel shows the original map obtained by the model, the other panels show the expected morphology after convolution with different beam sizes. The map expected at the ALMA resolution is shown in the bottom-left panel (c). In this model, the physical size of the torus is about 64 pc in diameter.

models.

The gas kinematics inferred from ALMA observations of the nuclear molecular emission lines will provide important information on the dynamical stability and origin of the circumnuclear medium. In the case of a simple uniform structure, supported by radiation pressure, we expect gas motions to be dominated mostly by rotation. In the case of a medium originated by the accretion disk wind (Elvis, 2000) we expect the molecular gas kinematics to also show a clear outflow component. In the case of a strong contribution by SN and stellar winds we also expect a strong turbulent component, hence a large width of the emission lines even within resolved regions. Obviously investigating the molecular gas in the innermost regions will require the observation of species typically tracing dense and highly excited gas (e.g. HCN, HCO<sup>+</sup>, ...), which are much fainter than CO, but easy to detect with ALMA. A detailed modelling of the excitation and emissivity distribution of these high density tracers in

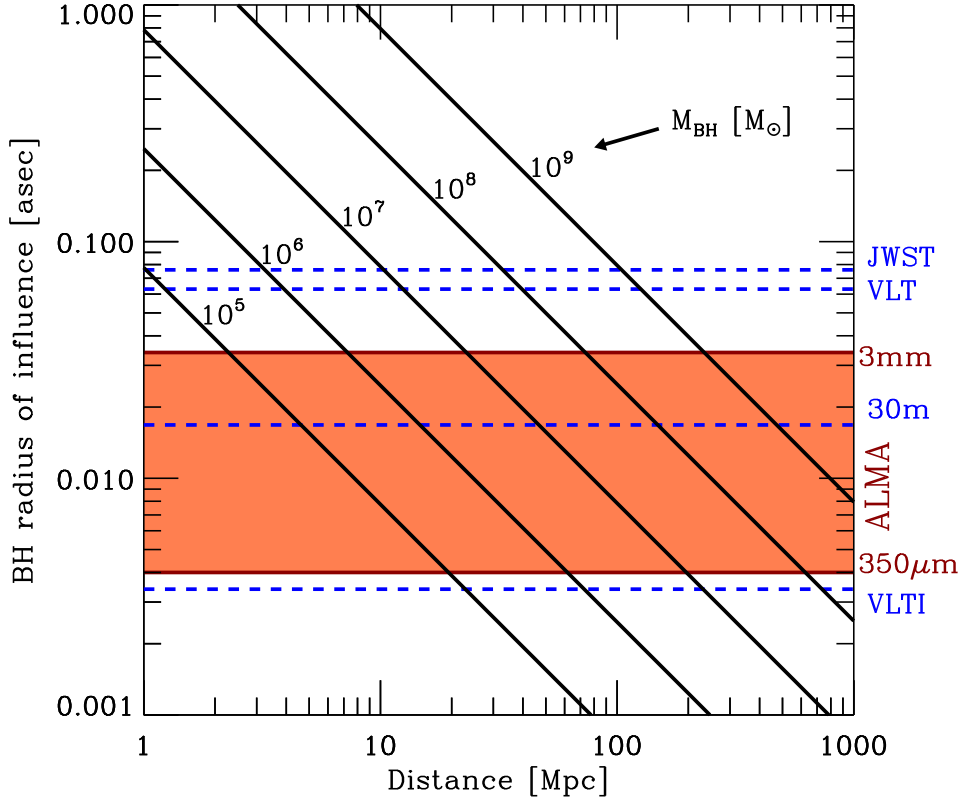


Fig. 16. Radius of influence (projected on the sky) of black holes of different masses as a function of the distance of their host galaxy. The radius of influence was calculated by assuming a stellar gravitational potential matching the  $M_{\text{BH}} - \sigma$  relation. The horizontal blue dashed lines indicate the angular resolution at  $\lambda = 2\mu\text{m}$  of various current or planned optical/near-IR facilities (JWST, 8m telescope, 30m telescope, VLTI). The red shaded area gives the range of angular resolution achievable with ALMA at different frequencies. Courtesy of A. Marconi.

AGN torii has been recently performed by Yamada et al. (2007). According to these models the flux ratios between these molecular lines is expected to be spatially highly inhomogeneous, reflecting the inhomogeneous structure of the molecular torus. Only the excellent angular resolution of ALMA will allow us to reveal such complex structures for the first time.

By resolving the molecular gas dynamics on such small scales it will be possible to measure the mass of the nuclear black hole. For instance, in NGC 1068 the  $10^7 M_{\odot}$  black hole has a sphere of influence with a radius of about 4 pc, requiring a beam projected on the sky smaller than  $0.05''$  to be resolved, which is achievable with ALMA at most frequencies. In NGC 1068, and a few additional nearby Sy2s, the BH mass has been already measured thanks to VLBI observations of a maser  $\text{H}_2\text{O}$  disk (Greenhill et al., 1996); however, the latter technique can only be exploited in a few cases where the maser disk is observed nearly edge-on (within  $15^\circ$  of the line of sight). ALMA observations of the nuclear molecular gas will allow us to extend the measurement of black

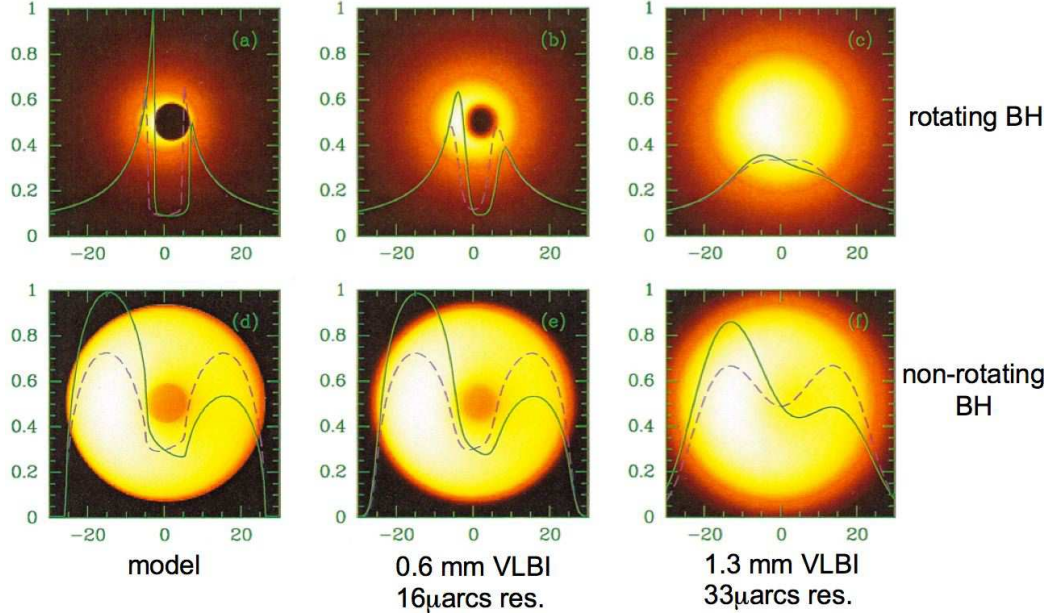


Fig. 17. Expected images of SgrA\* at mm-submm wavelengths with the angular resolution achievable with a mm-submm VLBI. The left panels illustrate the result of the model, showing a clear “shadow” due to the light bending by the gravitational field of the supermassive black hole. The other panels show the image obtained after convolution with the beam expected for the mm-submm VLBI. The panels on the top are for a rotating black hole, while the panels on the bottom are for a non-rotating black hole. From Falcke et al. (2000).

hole masses in AGNs to large samples, without stringent constraints on the geometry of the nuclear gas distribution. Fig. 16 shows the radius of influence, as projected on the sky, of black holes of different masses in the nuclei of galaxies, as a function of their distance (the central stellar gravitational potential is assumed to match the  $M_{\text{BH}} - \sigma$  relation). The red shaded area indicates the range of angular resolution achievable with ALMA at various frequencies. Clearly ALMA is in principle able to measure even very small black holes ( $M_{\text{BH}} < 10^5 M_{\odot}$ ) in nearby systems ( $D < 10$  Mpc); therefore ALMA will allow us to extend the investigation of the  $M_{\text{BH}} - \sigma$  relation to very low masses. ALMA will also allow us to measure massive black holes ( $M_{\text{BH}} > 10^7 M_{\odot}$ ) in distant systems,  $D \sim 50 - 1000$  Mpc; at these distances we can find the closest cases of merging systems (most of which are powerful ULIRGs). In these cases ALMA will measure the black hole mass within each of the two merging systems, which will allow us to place the two individual black holes on the  $M_{\text{BH}} - \sigma$  relation and to compare their location with the evolutionary path expected by models of hierarchical black hole growth (Dotti et al., 2007; Volonteri et al., 2003, e.g.).

ALMA will also be a powerful machine to discover heavily obscured AGNs. It is now clear that a population of obscured AGN are missed by optical spectroscopic surveys aimed at identifying AGNs through their characteristic nar-

row emission lines (Imanishi et al., 2007; Franceschini et al., 2003; Ballo et al., 2004; Caccianiga et al., 2007; Maiolino et al., 2003). Some of these obscured AGNs are missed because the Narrow Line Region is also obscured by dust in the host galaxy (Haas et al., 2005). In other cases the NLR is not formed at all (as inferred by the lack of NLR lines even in the mid-IR, Armus et al., 2007), probably because the ionizing radiation is absorbed in all directions (i.e.  $4\pi$  obscuration rather than a torus-like geometry). However, the X-rays emitted by the AGNs create extended XDRs, which are characterized by enhanced temperatures favoring the formation of several molecular species characteristics of these regions, as discussed in §2.1. The molecular transitions and diagnostics typical of these regions (e.g. enhanced HCN/HCO<sup>+</sup> Graciá-Carpio et al., 2006; Kohno et al., 2008) do not suffer any dust absorption and will be easily detected with ALMA even in distant systems. Therefore, ALMA will be able to provide an unbiased census of the AGN population, by including also those heavily obscured AGNs that are not detectable at other wavelengths.

I conclude this section by discussing the potentialities for the investigation of our Galactic center. The nuclear radio source SgrA\* is also a mm/submm source. If the emitting region is uniformly distributed around the supermassive black hole, then Falcke et al. (2000) showed that photons are expected to be deviated by the strong gravitational field within a few Schwarzschild radii, therefore creating a “shadow” in a putative mm/submm high resolution image (Fig. 17, left). There is a plan of combining ALMA with other mm/submm observatories distributed world wide to create (sub-)millimetric VLBI network, reaching an angular resolution of a few  $10\mu\text{arcsec}$ , which would allow us to resolve the black hole “shadow” (Fig. 17, right). This would really be a major result, essentially the first “picture” of a black hole. The shape and the contrast of the “shadow” would also allow us to determine whether the black hole is rotating (upper panels in Fig. 17) or not (lower panels).

## 5.2 High redshift galaxies and AGNs

We have seen in §2.3 that current mm/submm observations of high- $z$  objects are limited to very luminous systems ( $L_{\text{FIR}} \sim 10^{13} L_{\odot}$ ), not representative of the bulk of the galaxy population at high redshift. ALMA will be able to detect galaxies at least two orders of magnitude fainter, therefore providing an unbiased view of the evolution of galaxies from the mm/submm perspective. Fig. 5, compares the continuum sensitivity of ALMA (24 hours of integration) with the continuum flux expected by a galaxy with  $L_{\text{FIR}} = 10^{11} L_{\odot}$  (i.e.  $\text{SFR} \sim 15 M_{\odot} \text{ yr}^{-1}$ ) at various redshifts. It is clear that with the same integration time ALMA will be able to detect the thermal dust continuum of galaxies that are three times fainter. It is also interesting to note that for a SED typical of starburst galaxies the ALMA sensitivity nicely matches the mid/near-IR



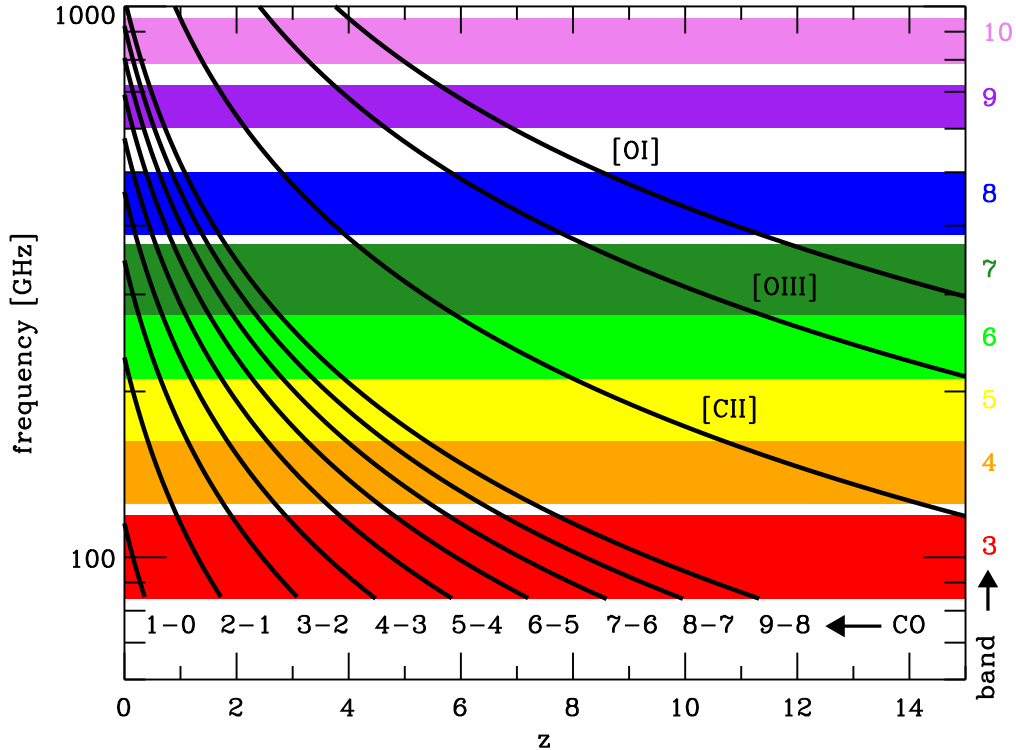


Fig. 18. Frequency of the various CO rotational transitions and of the [CII]158 $\mu$ m, [OI]63 $\mu$ m and [OIII]88 $\mu$ m fine structure lines as a function of redshift. The colored shaded bars indicate the frequency of the bands currently planned for ALMA.

sensitivity of JWST, another major facility which will be launched in 2013, i.e. when ALMA will be already fully operating. These two facilities will be fully complementary for the investigation of faint distant galaxies that are out of reach for current observatories.

Even in its compact configuration ALMA will have a resolution high enough ( $\sim 1''$ ) to make the confusion noise negligible, which is instead one of the main limitations of current surveys with single dish telescopes. The excellent ALMA resolution will allow astronomers to identify the optical/near-IR counterpart of mm-submm sources without ambiguities. The optical/near-IR counterpart may provide the redshift of the galaxy/AGN through optical/near-IR followup spectroscopy. However, ALMA will directly provide the redshift of the mm/submm sources through the detection of molecular lines or fine structure atomic lines. Fig. 18 shows the observed frequency of the CO rotational transitions as a function of redshift overlaid on the ALMA frequency bands. At  $z > 3$  at least two CO transitions are observable within band 3 (the most sensitive one), therefore unambiguously providing the redshift of the source. At  $z < 3$  the redshift confirmation requires the observation an additional CO line in a higher frequency band. Fig. 19 illustrates the ALMA sensitivity for the detection of the CO(6-5) line (which in SMGs is close to the peak of the CO lines intensities, Weiß et al., 2005b) for a galaxy with  $L_{\text{FIR}} = 10^{11} L_{\odot}$ .

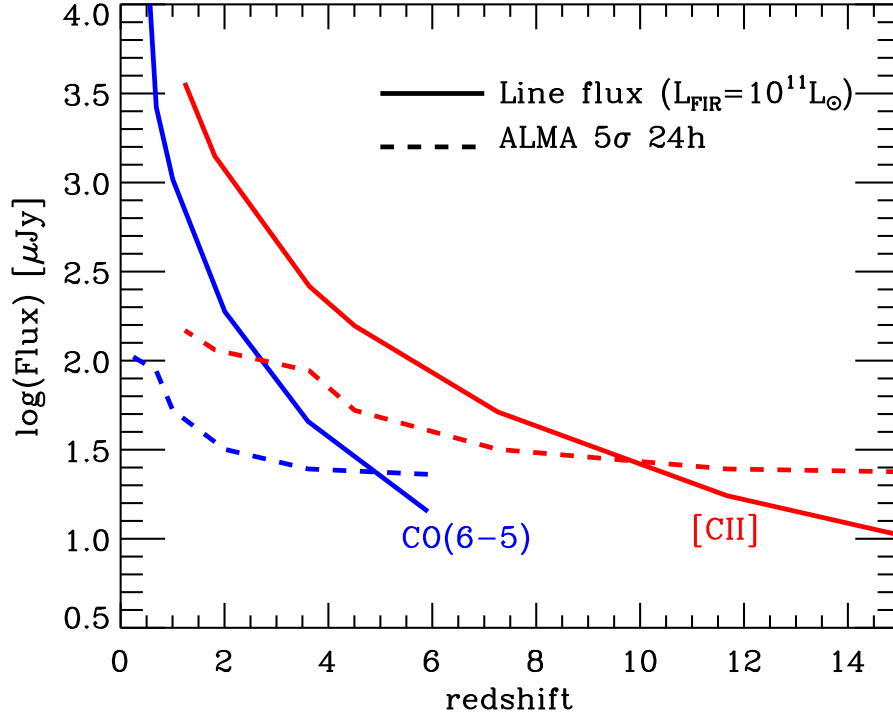


Fig. 19. *Solid lines:* CO(6–5) and [CII]158 $\mu$ m line fluxes expected for a galaxy with  $L_{\text{FIR}} = 10^{11} L_{\odot}$  as a function of redshift (keep in mind that the luminosity of these lines does not scale linearly with  $L_{\text{FIR}}$ ). *Dashed lines:* Sensitivity of ALMA (24 hours of integration) for a  $5\sigma$  detection of emission lines (width of 300 km/s) in the frequency bands corresponding to the CO(6–5) and [CII] redshifted lines. Here I have only considered the frequencies around the center of the bands and far from deep atmospheric absorption features (Tab. 3), and I have neglected band 5 (which has currently much lower sensitivity because available only for 6 antennas). The [CII] luminosity was inferred by fitting to the  $L_{\text{[CII]}}/L_{\text{FIR}}$  relation reported in Maiolino et al. (2005). The CO luminosity was inferred by assuming the  $L_{\text{CO}} - L_{\text{FIR}}$  relation in Fig.3 and by assuming the relative luminosities of the CO transitions observed in SMM J16359+6612 ( $z=2.5$ ) by Weiß et al. (2005b).

ALMA will clearly be able to detect this CO transition in Luminous Infrared Galaxies (LIRGs) out to  $z\sim 5$ . Note that to scale the diagram in Fig. 19 to other FIR luminosities one has to keep in mind the non-linear relation between  $L_{\text{CO}}$  and  $L_{\text{FIR}}$  (Fig. 3).

At  $z>7$  only CO transitions higher than (6–5) will be observable within the ALMA bands. However, such high transitions are generally little excited in most galaxies (Weiß et al., 2005b) and therefore more difficult to observe relative to the lower transitions. Yet, already at  $z>1$  the strong [CII]158 $\mu$ m line will be observable in the ALMA bands, and it will be one of the main tools to identify the redshift of distant sources, and in particular at  $z>7$  (Fig. 18). Fig. 19 shows that in LIRGs ( $L_{\text{FIR}} > 10^{11} L_{\odot}$ ) ALMA will be able to detect [CII] out to  $z\sim 10$ . Note that also in this case the diagram cannot be scaled

linearly to other FIR luminosities, since the relation between  $L_{[\text{CII}]}$  and  $L_{\text{FIR}}$  is not linear (Luhman et al., 2003).

The second brightest line is generally  $[\text{OI}]63\mu\text{m}$  (in some objects this line is even stronger than  $[\text{CII}]$ , but in some exceptional objects it may be self-absorbed).  $[\text{OI}]63\mu\text{m}$  will be observable at  $z > 4$  in the ALMA bands, and will help to obtain the redshift confirmation along with the  $[\text{CII}]$  detection. The  $[\text{OIII}]88\mu\text{m}$  line is also generally relatively strong, especially if an AGN is present ( $F_{[\text{OIII}]} \sim 0.5 - 0.3 F_{[\text{CII}]}$ ), and can be detected with ALMA at high redshifts. However, since  $[\text{OI}]$  and  $[\text{OIII}]$  will be observable at high- $z$  mostly in the high frequency bands, which are the least sensitive, the detection of these lines will probably be limited to ULIRGs (unless chemical evolutionary effects favor the emission of these oxygen lines, as discussed below).

The far-IR emission inferred from the mm/submm thermal continuum SED, along with the redshift inferred from the CO,  $[\text{CII}]$  and  $[\text{OI}]$  lines, will allow ALMA to provide a self-consistent, unbiased view of the evolution of the star formation rate through the cosmic epochs. For what concerns high- $z$  AGNs, ALMA will allow us to directly trace the coevolution of black hole growth (through the X-ray and optical emission) and of the formation of stellar mass in the host galaxies (through the far-IR emission). As discussed in §2.4, current mm/submm studies have found tentative indications of this co-evolution for very luminous systems ( $\text{SFR} \sim 1000 M_{\odot} \text{ yr}^{-1}$ ); ALMA will extend this investigation to much more quiescent systems ( $\text{SFR} \sim 10 M_{\odot} \text{ yr}^{-1}$ ), more representative of the bulk of the galaxy population at high redshift. The luminosity of the CO emission will provide the molecular gas mass for most of these galaxies and, when compared with the SFR, will provide a direct measure of the star formation efficiency (i.e. the star formation per unit gas mass) as a function of redshift.

In high redshift galaxies ( $z > 1$ ) the angular resolution of ALMA will allow us to resolve morphologies on sub-kpc scales. Besides providing the extension of the star formation activity and the distribution of the molecular gas, the ALMA maps will deliver precious information on the gas dynamics. By resolving rotation curves it will be possible to constrain the dynamical mass of individual galaxies, which can be compared with the expectations by hierarchical models of galaxy evolution. In the case of QSOs and type 1 AGNs it will be possible to directly compare the galaxy dynamical mass to the black hole mass (inferred from the broad optical/UV emission lines), therefore tracing any putative evolution of the  $M_{\text{BH}} - M_{\text{bulge}}$  relation. The observed evolution of the latter relation as a function of redshift will be directly comparable with the predictions of models dealing with the galaxy-BH co-evolution (Di Matteo et al., 2005; Granato et al., 2004; Dotti et al., 2007), and will therefore provide tight constraints on the same models.

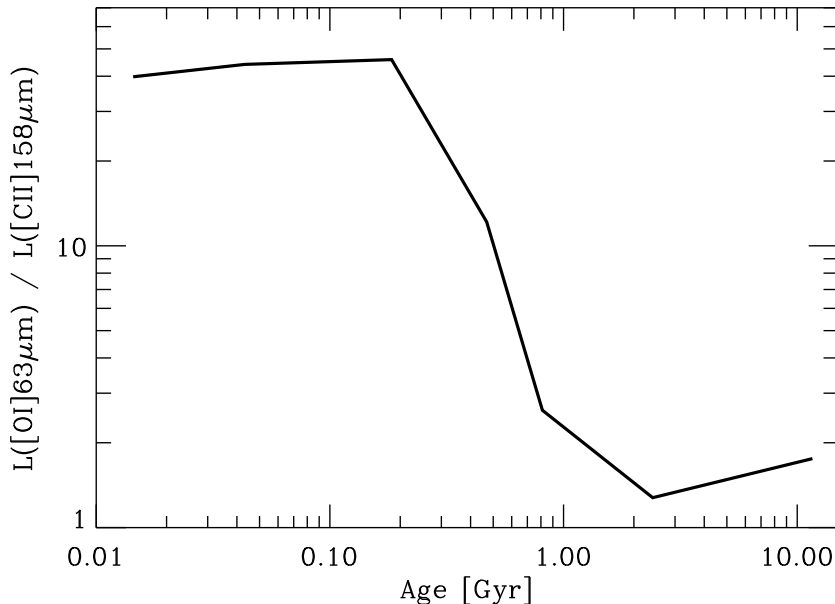


Fig. 20. Expected variation of the [OI]63 $\mu\text{m}$  to [CII]158 $\mu\text{m}$  intensity ratio as a function of galaxy age, by assuming the chemical evolutionary model in Pipino & Matteucci (2004). The model also assumes  $\log(U)=-2.5$ ,  $n = 10^3 \text{ cm}^{-3}$  and that the excitation conditions do not change over time. Courtesy of M. Kaufman.

The dynamics and morphology of the molecular gas will also provide information on the AGN fuelling mechanism. In §2.2 we saw that local AGNs do not show obvious systematic signatures of nuclear fuelling from the host galaxy, but also that such low luminosity AGNs do not actually require large fuelling from the host galaxy to maintain their low accretion rates. The fuelling demand from the host galaxy is however much larger in powerful QSOs, whose accretion rates may exceed a few  $M_{\odot} \text{ yr}^{-1}$ . Therefore, it is important to trace the dynamics of the molecular gas in the host of these powerful QSOs, and investigate for instance whether in these systems gas funneled by bars or driven by galaxy merging is common. However, such luminous QSOs are not found in the local universe, while are abundant at high redshift. Current facilities are in general unable to resolve the molecular gas dynamics in such distant systems, with very few exceptions. ALMA will allow us to trace in detail the gas dynamics in a large number of QSO hosts at high redshift and to statistically investigate the occurrence of various possible fuelling mechanisms. Detailed simulations are already being performed to assess the detectability and capability of resolving molecular gas morphologies in high- $z$  AGNs. Kawakatu et al. (2007) showed that not only ALMA will be able to resolve and detect the molecular gas in the host galaxy, but also the 100 pc gaseous torii expected to surround most of the supermassive black holes at  $z \sim 2$ .

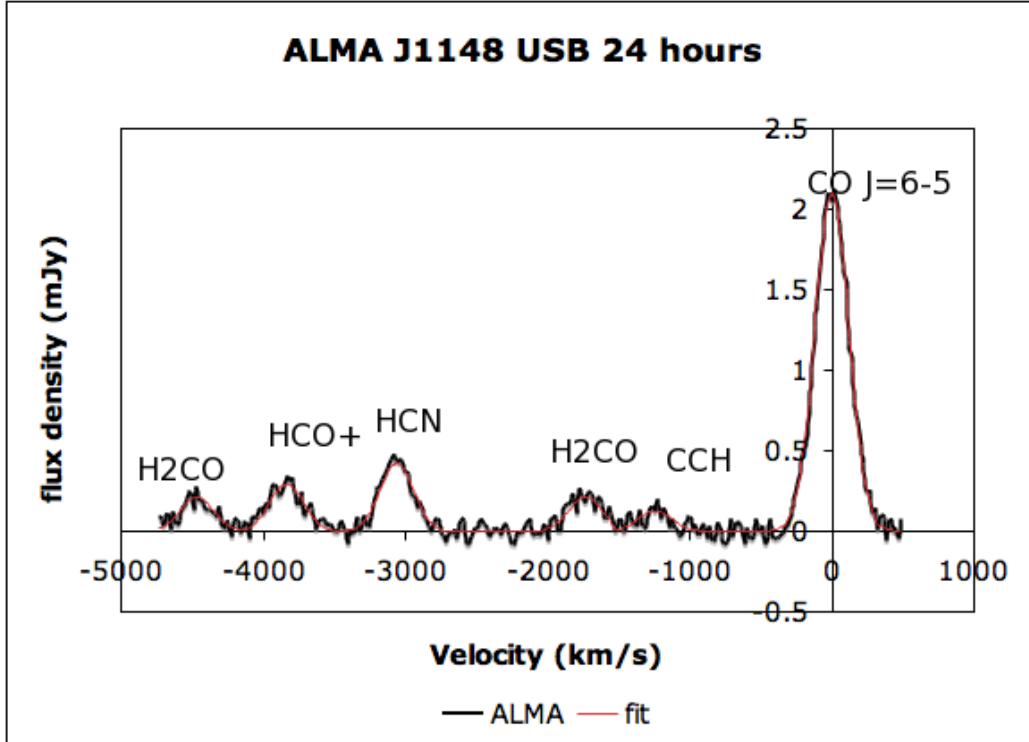


Fig. 21. Simulated ALMA spectrum (24 hours of integration) of a quasar with the same redshift ( $z=6.4$ ) and luminosity of the QSO J1148+5251, one of the most distant currently known. Courtesy of A. Wotten.

The ALMA detection of multiple molecular and atomic lines in high- $z$  galaxies and QSOs will also provide precious information on the chemical evolutionary status of the galaxy. For instance, the ratio of  $[\text{OI}]63\mu\text{m}$  and  $[\text{CII}]158\mu\text{m}$  is sensitive to the relative abundance of oxygen and carbon C/O. Since carbon is subject to a delayed enrichment with respect to oxygen (by several 100 Myr), the C/O abundance ratio is a sensitive tracer of the evolutionary stage of a galaxy. Fig. 20 shows the expected  $L_{[\text{OI}]63\mu\text{m}}/L_{[\text{CII}]158\mu\text{m}}$  ratio as a function of the age of a galaxy, by exploiting the chemical models in Pipino & Matteucci (2004) (the model assumes the physical conditions derived for the QSO at  $z=6.4$ , as discussed in Maiolino et al. (2005), and that the excitation conditions do not change over time). Therefore, by measuring both these lines, ALMA will allow us to constrain the evolutionary stage of distant galaxies. In particular, it will be extremely interesting to investigate the C/O abundance ratio in AGNs and galaxies at  $z\sim 7$ , close to the re-ionization epoch, where the age of the universe is close to the minimum enrichment timescale for carbon; at these redshifts the C/O ratio is expected to be very low, and therefore the  $[\text{OI}]/[\text{CII}]$  ratio is expected to be very high.

In very luminous high- $z$  sources, such as the QSOs already detected with current facilities, ALMA will be able to easily detect several other molecular (e.g. HCN,  $\text{HCO}^+$ , ...) and atomic (e.g.  $[\text{NII}]122\mu\text{m}$ ) transitions, which will

allow us to perform an accurate modelling of the physics of the ISM and to infer accurate chemical abundances (hence the evolutionary stage of the system). As an example, Fig. 21 shows the simulated ALMA spectrum (24 hours of integration) of a quasar with the same redshift ( $z=6.4$ ) and luminosity of the QSO J1148+5251, which is currently the most distant QSO with a CO detection. Beside the CO(6–5) transition, the 8 GHz ALMA band is expected to reveal several other molecular transitions with excellent signal-to-noise.

Finally, ALMA will allow us to investigate in detail the evolution of dust production in the early universe. The dust mass in galaxies can only be inferred by measuring the (rest-frame) infrared to submm SED. Currently dust masses have been measured only for very powerful systems at high- $z$  (QSOs and SMGs), providing an incomplete and very biased view, not representative of the global evolution of dust through the cosmic epochs. ALMA will measure the dust mass in large samples of high- $z$  systems, even in relatively quiescent ones (SFR of a few  $M_{\odot} \text{ yr}^{-1}$ ). Therefore, it will be possible to trace the evolution of dust mass as a function of redshift and for different classes of galaxies, which can be directly compared with models of dust evolution (Morgan & Edmunds, 2003; Dwek et al., 2007; Calura et al., 2008). In particular, it will be important to clarify whether dust produced by SNe can actually be the main source of dust in the early universe, or whether other mechanisms of dust production are required (Dwek et al., 2007; Elvis et al., 2002).

I am grateful to the organizers of the school for their kind invitation. I thank M. Walmsley, P. Caselli, K. Wada and L. Testi for many useful comments on the manuscript. I am grateful to C. Dowell, A. Beelen, A. Marconi, M. Kaufman and A. Wotten for providing some of the figures in these lecture notes. Some of the images were reproduced with kind permission of the Space Telescope Science Institute and of the European Southern Observatory. Finally, I acknowledge financial support by the National Institute for Astrophysics (INAF) and by the Italian Space Agency (ASI).

## References

- Alexander, D. M., et al. 2003, *AJ*, 125, 383  
Alexander, D. M., Bauer, F. E., Chapman, S. C., Smail, I., Blain, A. W., Brandt, W. N., & Ivison, R. J. 2005, *ApJ*, 632, 736  
Armus, L., et al. 2007, *ApJ*, 656, 148  
Ballo, L., Braitto, V., Della Ceca, R., Maraschi, L., Tavecchio, F., & Dadina, M. 2004, *ApJ*, 600, 634  
Beelen, A., Cox, P., Benford, D. J., Dowell, C. D., Kovács, A., Bertoldi, F., Omont, A., & Carilli, C. L. 2006, *ApJ*, 642, 694  
Bertoldi, F., Carilli, C. L., Cox, P., Fan, X., Strauss, M. A., Beelen, A., Omont, A., & Zylka, R. 2003a, *A&A*, 406, L55

- Bertoldi, F., et al. 2003b, *A&A*, 409, L47
- Blain, A. W., Smail, I., Ivison, R. J., Kneib, J.-P., & Frayer, D. T. 2002, *Physics Reports*, 369, 111
- Caccianiga, A., Severgnini, P., Della Ceca, R., Maccacaro, T., Carrera, F. J., & Page, M. J. 2007, *A&A*, 470, 557
- Calura, F., Pipino, A., Matteucci, F., & - 2008, *ArXiv e-prints*, 801, arXiv:0801.2551
- Carilli, C. L., et al. 2001, *ApJ*, 555, 625
- Carilli, C. L., et al. 2005, *ApJ*, 618, 586
- Carilli, C. L., & Wang, R. 2006, *AJ*, 131, 2763
- Chapman, S. C., Blain, A. W., Smail, I., & Ivison, R. J. 2005, *ApJ*, 622, 772
- Combes, F., et al. 2004, *A&A*, 414, 857
- Daddi, E., Dannerbauer, H., Elbaz, D., Dickinson, M., Morrison, G., Stern, D., & Ravindranath, S. 2008, *ApJ*, 673, L21
- De Breuck, C., Downes, D., Neri, R., van Breugel, W., Reuland, M., Omont, A., & Ivison, R. 2005, *A&A*, 430, L1
- Di Matteo, T., Springel, V., & Hernquist, L. 2005, *Nature*, 433, 604
- Dotti, M., Colpi, M., Haardt, F., & Mayer, L. 2007, *MNRAS*, 379, 956
- Dwek, E., Galliano, F., & Jones, A. P. 2007, *ApJ*, 662, 927
- Elitzur, M., & Shlosman, I. 2006, *ApJ*, 648, L101
- Elvis, M. 2000, *ApJ*, 545, 63
- Elvis, M., Marengo, M., & Karovska, M. 2002, *ApJ*, 567, L107
- Erickson et al. 2007, in “From Z-Machines to ALMA: (Sub)millimeter Spectroscopy of Galaxies” *ASP Conf. Series*
- Falcke, H., Melia, F., & Agol, E. 2000, *ApJ*, 528, L13
- Ferrarese, L., & Merritt, D. 2000, *ApJ*, 539, L9
- Franceschini, A., et al. 2003, *MNRAS*, 343, 1181
- Gao, Y., Carilli, C. L., Solomon, P. M., & Vanden Bout, P. A. 2007, *ApJ*, 660, L93
- García-Burillo, S., Combes, F., Schinnerer, E., Boone, F., & Hunt, L. K. 2005, *A&A*, 441, 1011
- García-Burillo, S., et al. 2006, *ApJ*, 645, L17
- García-Burillo, S., Combes, F., Usero, A., & Graciá-Carpio, J. 2007, *New Astronomy Review*, 51, 160
- Gebhardt, K., et al. 2000, *ApJ*, 539, L13
- Genzel, R., Baker, A. J., Tacconi, L. J., Lutz, D., Cox, P., Guilloteau, S., & Omont, A. 2003, *ApJ*, 584, 633
- Genzel, R., et al. 2005, *Multiwavelength Mapping of Galaxy Formation and Evolution*, 112
- Glenn, J., et al. 2007, in “From Z-Machines to ALMA: (Sub)millimeter Spectroscopy of Galaxies” *ASP Conf. Series*
- Graciá-Carpio, J., García-Burillo, S., Planesas, P., & Colina, L. 2006, *ApJ*, 640, L135
- Graciá-Carpio, J., García-Burillo, S., Planesas, P., Fuente, A., & Usero, A. 2008, *A&A*, 479, 703

- Granato, G. L., De Zotti, G., Silva, L., Bressan, A., & Danese, L. 2004, *ApJ*, 600, 580
- Greenhill, L. J., Gwinn, C. R., Antonucci, R., & Barvainis, R. 1996, *ApJ*, 472, L21
- Greve, T. R., et al. 2005, *MNRAS*, 359, 1165
- Guélin, M., et al. 2007, *A&A*, 462, L45
- Harris, A.I., et al. 2007, in “From Z-Machines to ALMA: (Sub)millimeter Spectroscopy of Galaxies” ASP Conf. Series
- Haas, M., Siebenmorgen, R., Schulz, B., Krügel, E., & Chini, R. 2005, *A&A*, 442, L39
- Helfer, T. T., Thornley, M. D., Regan, M. W., Wong, T., Sheth, K., Vogel, S. N., Blitz, L., & Bock, D. C.-J. 2003, *ApJS*, 145, 259
- Ho, L. C. 2007, *ApJ*, 669, 821
- Hönig, S. F., Beckert, T., Ohnaka, K., & Weigelt, G. 2006, *A&A*, 452, 459
- Imanishi, M., Dudley, C. C., Maiolino, R., Maloney, P. R., Nakagawa, T., & Risaliti, G. 2007, *ApJS*, 171, 72
- Iono, D., et al. 2006, *ApJ*, 645, L97
- Isaak, K. G., Priddey, R. S., McMahon, R. G., Omont, A., Peroux, C., Sharp, R. G., & Withington, S. 2002, *MNRAS*, 329, 149
- Jaffe, W., et al. 2004, *Nature*, 429, 47
- Kawakatu, N., Andreani, P., Granato, G. L., & Danese, L. 2007, *ApJ*, 663, 924
- Kneib, J.-P., Alloin, D., Mellier, Y., Guilleaume, S., Barvainis, R., & Antonucci, R. 1998, *A&A*, 329, 827
- Kohno, K., Nakanishi, K., Tosaki, T., Muraoka, K., Miura, R., Ezawa, H., & Kawabe, R. 2008, *AP&SS*, 313, 279
- Krolik, J. H. 2007, *ApJ*, 661, 52
- Lepp, S., & Dalgarno, A. 1996, *A&A*, 306, L21
- Lewis, G. F., Carilli, C., Papadopoulos, P., & Ivison, R. J. 2002, *MNRAS*, 330, L15
- Luhman, M. L., Satyapal, S., Fischer, J., Wolfire, M. G., Sturm, E., Dudley, C. C., Lutz, D., & Genzel, R. 2003, *ApJ*, 594, 758
- Lutz, D., et al. 2007, *ApJ*, 661, L25
- Lutz, D., et al. 2008, *ApJ*, in press
- Maiolino, R., et al. 2003, *MNRAS*, 344, L59
- Maiolino, R., Schneider, R., Oliva, E., Bianchi, S., Ferrara, A., Mannucci, F., Pedani, M., & Roca Sogorb, M. 2004, *Nature*, 431, 533
- Maiolino, R., et al. 2005, *A&A*, 440, L51
- Maiolino, R., Shemmer, O., Imanishi, M., Netzer, H., Oliva, E., Lutz, D., & Sturm, E. 2007a, *A&A*, 468, 979
- Maiolino, R., et al. 2007b, *A&A*, 472, L33
- Maiolino, R., & Risaliti, G. 2007, *The Central Engine of Active Galactic Nuclei*, 373, 447
- Marconi, A., & Hunt, L. K. 2003, *ApJ*, 589, L21
- Matt, G., et al. 1997, *A&A*, 325, L13



- McLure, R. J., Jarvis, M. J., Targett, T. A., Dunlop, J. S., & Best, P. N. 2006, MNRAS, 368, 1395
- Meijerink, R., Spaans, M., & Israel, F. P. 2007, A&A, 461, 793
- Menéndez-Delmestre, K., et al. 2007, ApJ, 655, L65
- Maloney, P. R., Hollenbach, D. J., & Tielens, A. G. G. M. 1996, ApJ, 466, 561
- Morgan, H. L., & Edmunds, M. G. 2003, MNRAS, 343, 427
- Nayakshin, S., & Cuadra, J. 2007, A&A, 465, 119
- Nenkova, M., Ivezić, Ž., & Elitzur, M. 2002, ApJ, 570, L9
- Netzer, H., et al. 2007, ApJ, 666, 806
- Nozawa, T., Kozasa, T., Umeda, H., Maeda, K., & Nomoto, K. 2003, ApJ, 598, 785
- Omont, A., Petitjean, P., Guilloteau, S., McMahon, R. G., Solomon, P. M., & Pécontal, E. 1996, Nature, 382, 428
- Omont, A., Beelen, A., Bertoldi, F., Cox, P., Carilli, C. L., Priddey, R. S., McMahon, R. G., & Isaak, K. G. 2003, A&A, 398, 857
- Omont, A. 2007, Reports of Progress in Physics, 70, 1099
- Papadopoulos, P. P., Röttgering, H. J. A., van der Werf, P. P., Guilloteau, S., Omont, A., van Breugel, W. J. M., & Tilanus, R. P. J. 2000, ApJ, 528, 626
- Papadopoulos, P. P. 2007, ApJ, 656, 792
- Peng, C. Y., Impey, C. D., Rix, H.-W., Kochanek, C. S., Keeton, C. R., Falco, E. E., Lehár, J., & McLeod, B. A. 2006, ApJ, 649, 616
- Pipino, A., & Matteucci, F. 2004, MNRAS, 347, 968
- Pope, A., et al. 2008, ApJ, 675, 1171
- Priddey, R. S., Isaak, K. G., McMahon, R. G., Robson, E. I., & Pearson, C. P. 2003, MNRAS, 344, L74
- Regan, M. W., Sheth, K., & Vogel, S. N. 1999, ApJ, 526, 97
- Rho, J., et al. 2008, ApJ, 673, 271
- Riechers, D. A., Walter, F., Carilli, C. L., Weiss, A., Bertoldi, F., Menten, K. M., Knudsen, K. K., & Cox, P. 2006, ApJ, 645, L13
- Riechers, D. A., Walter, F., Carilli, C. L., & Bertoldi, F. 2007, ApJ, 671, L13
- Schinnerer, E., Eckart, A., Tacconi, L. J., Genzel, R., & Downes, D. 2000, ApJ, 533, 850
- Schinnerer, E., Böker, T., Emsellem, E., & Downes, D. 2007, A&A, 462, L27
- Schweitzer, M., et al. 2006, ApJ, 649, 79
- Smail, I. 2006, ArXiv Astrophysics e-prints, arXiv:astro-ph/0603635
- Solomon, P. M., & Vanden Bout, P. A. 2005, ARA&A, 43, 677
- Stacey, G.J., et al. 2007, in “From Z-Machines to ALMA: (Sub)millimeter Spectroscopy of Galaxies” ASP Conf. Series
- Stratta, G., Maiolino, R., Fiore, F., & D’Elia, V. 2007, ApJ, 661, L9
- Sugerman, B. E. K., et al. 2006, Science, 313, 196
- Tacconi, L. J., Genzel, R., Blietz, M., Cameron, M., Harris, A. I., & Madden, S. 1994, ApJ, 426, L77
- Tacconi, L. J., et al. 2006, ApJ, 640, 228
- Tacconi, L. J., et al. 2008, ApJ, in press (arXiv:0801.3650v1)
- Todini, P., & Ferrara, A. 2001, MNRAS, 325, 726

- Usero, A., García-Burillo, S., Fuente, A., Martín-Pintado, J., & Rodríguez-Fernández, N. J. 2004, *A&A*, 419, 897
- Valiante, E., Lutz, D., Sturm, E., Genzel, R., Tacconi, L. J., Lehnert, M. D., & Baker, A. J. 2007, *ApJ*, 660, 1060
- Venturini, S., & Solomon, P. M. 2003, *ApJ*, 590, 740
- Volonteri, M., Haardt, F., & Madau, P. 2003, *ApJ*, 582, 559
- Wada, K., & Tomisaka, K. 2005, *ApJ*, 619, 93
- Wagg, J., Wilner, D. J., Neri, R., Downes, D., & Wiklind, T. 2005, *ApJ*, 634, L13
- Walter, F., et al. 2003, *Nature*, 424, 406
- Walter, F., Carilli, C., Bertoldi, F., Menten, K., Cox, P., Lo, K. Y., Fan, X., & Strauss, M. A. 2004, *ApJ*, 615, L17
- Wang, R., et al. 2007, *AJ*, 134, 617
- Wang, R., et al. 2008, *AJ*, 135, 1201
- Watabe, Y., & Umemura, M. 2005, *ApJ*, 618, 649
- Wei, A., Downes, D., Henkel, C., & Walter, F. 2005a, *A&A*, 429, L25
- Wei, A., Downes, D., Walter, F., & Henkel, C. 2005b, *A&A*, 440, L45
- Wei, A., Downes, D., Neri, R., Walter, F., Henkel, C., Wilner, D. J., Wagg, J., & Wiklind, T. 2007, *A&A*, 467, 955
- Willott, C. J., et al. 2007, *AJ*, 134, 2435
- Wu, J., Evans, N. J., II, Gao, Y., Solomon, P. M., Shirley, Y. L., & Vanden Bout, P. A. 2005, *ApJ*, 635, L173
- Wu, X.-B. 2007, *ApJ*, 657, 177
- Yamada, M., Wada, K., & Tomisaka, K. 2007, *ApJ*, 671, 73